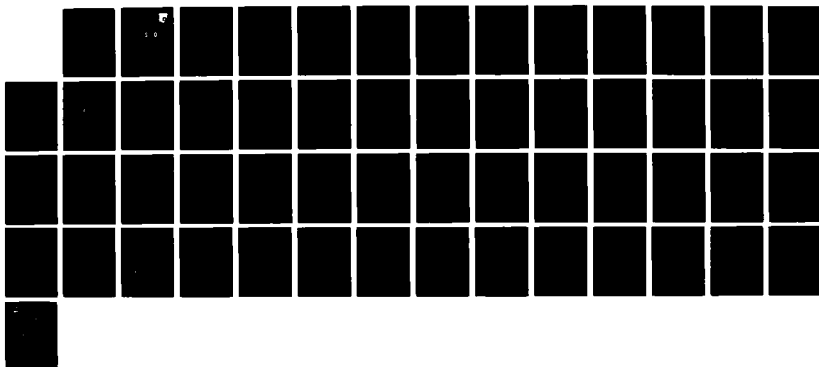
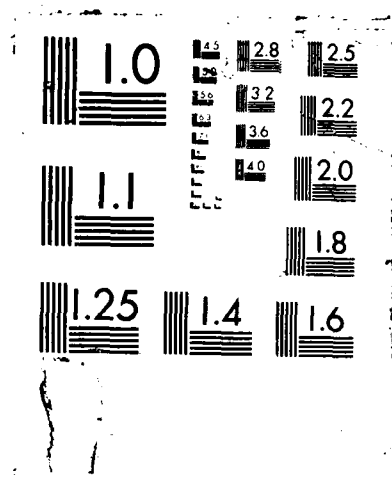


AD-A189 274 AN ELECTROCHEMICAL AND SPECTROSCOPIC STUDY OF ELECTRODE 1/1
SYSTEMS(U) DAYTON UNIV OH RESEARCH INST
R G KEIL ET AL SEP 87 AFWAL-TR-87-2047
UNCLASSIFIED F33615-86-C-2620 F/G 7/4 NL





AD-A189 274

DTIC FILE COPY

2

AFWAL-TR-87-2047

AN ELECTROCHEMICAL AND SPECTROSCOPIC
STUDY OF ELECTRODE SYSTEMS



R. G. Keil and S. P. Sinha

University of Dayton
Research Institute
300 College Park
Dayton, Ohio 45469-0001

DTIC
ELECTE
JAN 28 1988
S D

September 1987

Final Report for Period May 1986 - January 1987

Approved for public release; distribution is unlimited.

AERO PROPULSION LABORATORY
AIR FORCE WRIGHT AERONAUTICAL LABORATORIES
AIR FORCE SYSTEMS COMMAND
WRIGHT-PATTERSON AIR FORCE BASE, OHIO 45433-6563

NOTICE

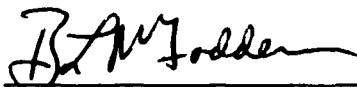
When Government drawings, specifications, or other data are used for any purpose other than in connection with a definitely related Government procurement operation, the United States Government thereby incurs no responsibility nor any obligation whatsoever; and the fact that the government may have formulated, furnished, or in any way supplied the said drawings, specifications, or other data, is not to be regarded by implication or otherwise as in any manner licensing the holder or any other person or corporation, or conveying any rights or permission to manufacture use, or sell any patented invention that may in any way be related thereto.

This report is releasable to the National Technical Information Service (NTIS). At NTIS, it will be available to the general public, including foreign nations.

This technical report has been reviewed and is approved for publication.

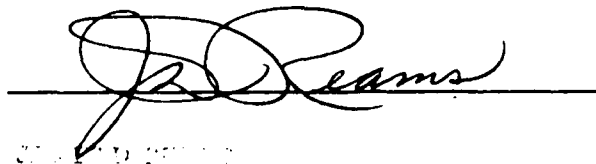


RICHARD A. MARSH, Acting TAM
Batteries and Fuel Cells



BURYL L. MCFADDEN, Chief
Power Technology Branch
Aerospace Power Division
Aero Propulsion Laboratory

FOR THE COMMANDER



J. D. REAMS
Chief, Aerospace Power Division
Aero Propulsion Laboratory

If your address has changed, if you wish to be removed from our mailing list, or if the addressee is no longer employed by your organization please notify AFWAL/POOS-2 W-PAFB, OH 45433 to help us maintain a current mailing list.

Copies of this report should not be returned unless return is required by security considerations, contractual obligations, or notice on a specific document.

UNCLASSIFIED

SECURITY CLASSIFICATION OF THIS PAGE

REPORT DOCUMENTATION PAGE				Form Approved OMB No. 0704-0188	
1a. REPORT SECURITY CLASSIFICATION UNCLASSIFIED			1b. RESTRICTIVE MARKINGS None		
2a. SECURITY CLASSIFICATION AUTHORITY			3. DISTRIBUTION / AVAILABILITY OF REPORT Approval for public release: distribution unlimited		
2b. DECLASSIFICATION / DOWNGRADING SCHEDULE					
4. PERFORMING ORGANIZATION REPORT NUMBER(S)			5. MONITORING ORGANIZATION REPORT NUMBER(S) AFWAL-TR-87-2047		
6a. NAME OF PERFORMING ORGANIZATION University of Dayton Research Institute		6b. OFFICE SYMBOL (If applicable)	7a. NAME OF MONITORING ORGANIZATION Air Force Wright Aeronautical Laboratories Aero Propulsion Laboratory (AFWAL/POO5-2)		
6c. ADDRESS (City, State, and ZIP Code) 300 College Park Ave. Dayton, Ohio 45469-0001		7b. ADDRESS (City, State, and ZIP Code) Wright-Patterson AFB, Ohio 45433-6563			
8a. NAME OF FUNDING / SPONSORING ORGANIZATION AF Office of Scientific Research		8b. OFFICE SYMBOL (If applicable)	9. PROCUREMENT INSTRUMENT IDENTIFICATION NUMBER F33615-86-C-2620		
8c. ADDRESS (City, State, and ZIP Code) Bolling AFB Washington DC		10. SOURCE OF FUNDING NUMBERS			
		PROGRAM ELEMENT NO. 61102F	PROJECT NO. 2303	TASK NO. S4	WORK UNIT ACCESSION NO. 10
11. TITLE (Include Security Classification) An Electrochemical and Spectroscopic Study of Electrode Systems					
12. PERSONAL AUTHOR(S) R. G. Keil and Sh ³ P. Sinha					
13a. TYPE OF REPORT Final		13b. TIME COVERED FROM 5/86 TO 1/87		14. DATE OF REPORT (Year, Month, Day) 87 September	
15. PAGE COUNT 55					
16. SUPPLEMENTARY NOTATION					
17. COSATI CODES			18. SUBJECT TERMS (Continue on reverse if necessary and identify by block number)		
FIELD	GROUP	SUB-GROUP	Electrochemistry, Spectroscopy, Batteries ←		
09	01				
10	03				
19. ABSTRACT (Continue on reverse if necessary and identify by block number)					
<p>This final report concerns research in the area of electrochemical and spectroscopic studies on electrode and electrolyte systems for use within nonaqueous battery systems from 1 May 1986 through 31 January, 1987.</p> <p>The research has as a unifying theme the use of electrochemical and spectroscopic methods in the pursuit of an understanding of the chemical processes which occur at the electrodes as well as within the solution phase. The work is divided into two distinct phases: (a) the study of imidazolium melts and (b) the electrochemical reversibility of lithium.</p> <p><i>(Key)</i></p>					
20. DISTRIBUTION / AVAILABILITY OF ABSTRACT <input checked="" type="checkbox"/> UNCLASSIFIED/UNLIMITED <input type="checkbox"/> SAME AS RPT <input type="checkbox"/> DTIC USERS			21. ABSTRACT SECURITY CLASSIFICATION Unclassified		
22a. NAME OF RESPONSIBLE INDIVIDUAL David H. Fritts			22b. TELEPHONE (Include Area Code) 255-2372 (513)		22c. OFFICE SYMBOL AFWAL/POOS-2

TABLE OF CONTENTS

<u>SECTION</u>	<u>PAGE</u>
I METHYL-ETHYL IMIDAZOLIUM CHLORIDE ALUMINUM CHLORIDE MELTS	1
1.1 Preparation and Purification of MEIC	1
1.2 Preparation of the Melt	2
1.3 Identification of the Melts	3
1.3.1 UV/VIS Spectra	3
1.3.2 Infrared and Raman Spectra	5
1.3.3 Fluorescence Spectra	9
II ELECTROCHEMISTRY	14
2.1 Electrochemistry of Cerium	14
2.2 Electrochemistry of Uranium	18
2.3 Electrochemistry of Terbium	24
2.4 Electrochemistry of Aqueous Solutions	25
2.5 Summary of Results	25
2.6 Scope of Further Studies	26
References	26
III LITHIUM ELECTROCHEMISTRY IN ACETONITRILE: AN ELECTROCHEMICAL AND SPECTROSCOPIC STUDY OF ELECTRODE SYSTEMS	30
3.1 Introduction	30
3.2 Preparation and Characterization of Solvent-Electrolytes	31
3.3 The Electrochemistry of Lithium	34
IV SUMMARY OF RESULTS	38
4.1 Suggestions for Future Research	38
References	38
V REFERENCES	39
APPENDIX	A-1
Hexachloro Complex of Uranium(V) in Room Temperature Ionic Melt	A-1
Resistive Electrode Effects on Cyclic Voltammetry	A-3

LIST OF FIGURES

<u>FIGURE</u>		<u>PAGE</u>
1	UV/VIS Spectra of MEIC-AlCl ₃ Melts Containing Various Mole Fractions(N) of AlCl ₃ .	4
2	Infrared Spectra of (a) 0.4 Melt, (b) 0.6 Melt and (c) 0.4 Melt Containing CeCl ₃ .	7
3	Raman Spectrum of a 0.33 Chloroaluminate (MEIC-AlCl ₃) Melt at Room Temperature	10
4	Raman Spectrum of a 0.66 Chloroaluminate (MEIC-AlCl ₃) Melt at Room Temperature	11
5	Excitation and Fluorescence Spectra of 0.4 Chloroaluminate (MEIC-AlCl ₃) Melt at Room Temperature	13
6	Cyclic Voltammogram of 0.4 Chloroaluminate (MEIC-AlCl ₃) Melt at Room Temperature, 50 mV per Sec.; (A) One Microamp per Inch, (B) 10 Microamp per Inch	15
7	Cyclic Voltammogram of 0.4 Chloroaluminate (MEIC-AlCl ₃) Melt Containing CeCl ₃ , Showing Quasi-Reversible Behavior	17
8	Fluorescence and Excitation Spectra of Ce(III) in a 0.4 MEIC-AlCl ₃ Melt	19
9	Ultraviolet Spectrum of the "Yellow" Solution of UCl ₄ in 0.4 MEIC-AlCl ₃ Melt Showing the Electron Transfer Transitions of U(V) Species	21
10	Cyclic Voltammetry of the "Yellow" U(V) Species Which Results from the Oxidation of a UCl ₄ Solution in 0.4 MEIC-AlCl ₃ Melt. Notice that the Anodic Peak is much Weaker than the Cathodic	22
11	Cyclic Voltammetry of an Aqueous Solution of Eu(III) in 1m Chloride	27
12	Cyclic Voltammetry of an Aqueous Solution of Sm(III) in 1m Chloride	28
13	(a) Typical Capillary Column Gas Chromatograph of Acetonitrile Showing Trace Impurity of Propionitrile. (b) Ultraviolet Spectra of Acetonitrile Samples: (A) Fisher, (B) Burdick and Jackson, and (C) Alfa	33

LIST OF FIGURES
(Concluded)

<u>FIGURE</u>		<u>PAGE</u>
14	Cyclic Voltammogram of TBATFB in Acetonitrile at Platinum, 200mV/sec, Zero to Minus 2.5 Volts, Silver Reference Electrode, as a Function of Current Sensitivity	35
15	Cyclic Voltammogram of TBATFB and Lithium Perchlorate in Acetonitrile at Platinum, 100mV/Sec, Zero to Minus 2.6 Volts, 2.5 Microamp per inch, Silver Reference, Multiple Scan	36

Accession For	
NTIS CRA&I	<input checked="" type="checkbox"/>
DTIC TAB	<input type="checkbox"/>
Unannounced	<input type="checkbox"/>
Justification	
By	
Distribution	
Availability Codes	
Dist	Avail. and/or Special
A-1	

LIST OF TABLES

<u>TABLE</u>		<u>PAGE</u>
1	Ultraviolet Data on MEIC-AlCl_3 Room Temperature Melts	6
2	Infrared Analysis of the Tetrachloroaluminate Ion	8
3	Details of Cyclic Voltammetric Data on "Yellow" UCl_6^- Solution in 0.4 Melt	23

SECTION I

METHYL-ETHYL IMIDAZOLIUM CHLORIDE ALUMINUM CHLORIDE MELTS

The family of ambient temperature melts which result from mixtures of 1,3-dialkylimidazolium chloride and aluminum chloride was discovered at the Frank J. Siler Laboratories. The most extensively investigated room-temperature melt consists of 1-methyl-3-ethylimidazolium chloride(I) and aluminum chloride in various mole ratios. These melts have interesting properties which include: low liquid temperature, anhydrous aprotic solvent, large electrochemical window and good conductivity. We desire to prepare, characterize, identify these melts and to study their electrochemical and spectroscopic properties. Of particular interest are the redox properties of various lanthanide elements.

1.1 PREPARATION AND PURIFICATION OF MEIC

1-methylimidazole was reacted with ethylchloride, by condensing the gas within a pressure bottle at 45 degrees centigrade for a period of a week with occasional shaking. The use of both a lower reaction temperature and a longer reaction time resulted in a higher yield^(1,2) of the desired product, MEIC. Evidence of the formation of the solid MEIC usually appears after a time period of a week with occasional shaking. The use of both a lower reaction temperature and a longer reaction time resulted in a higher yield of the desired product, MEIC. Evidence of the formation of the solid MEIC usually appears after a time period

of three days under these reaction conditions. At the end of the reaction period, the pressure bottle was allowed to cool to near room temperature and subsequently cooled further within an ice bath. CAUTION must be exercised here because there is usually a residual positive pressure within the reaction vessel and care should be exercised in opening the neoprene stopper. The small amount of liquid remaining within the bottle was poured off and discarded in a well ventilated hood. The pressure bottle was stoppered with a Calcium chloride drying tube and warmed to a temperature of 40 degrees centigrade until all visible signs of remaining ethyl chloride were removed.

The purification of MEIC was carried out as follows. MEIC was purified twice from acetonitrile/ethylacetate and ethyl ether mixture. All experiments were carried out under an atmosphere of dry nitrogen. Solvent removal and further purification were achieved under vacuum. Aluminum trichloride was usually purified by sublimation of 5 N's pure material obtained from Alfa Products.

1.2 PREPARATION OF THE MELT

Reaction of MEIC and aluminum chloride is highly exothermic. Caution should be taken during melt preparation. Small quantities of the melt (50 grams) were prepared by slowly adding aluminum chloride in small portions to a weighed amount of MEIC in a nitrogen atmosphere. Melts of various compositions were prepared and compositions were usually expressed in terms of the

mole fraction of aluminum chloride present. The following terminology was used:

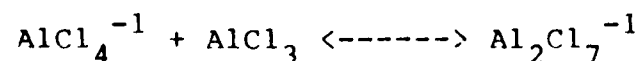
MEIC/ AlCl_3 mole ratio 0.6/0.4 or 0.4 melt (basic)
0.5/0.5 or 0.5 melt (neutral)
0.4/0.6 or 0.6 melt (acidic)

Melts which were to contain metal ions were prepared by dissolving anhydrous lanthanide or uranium chloride salts therein.

1.3 IDENTIFICATION OF THE MELTS

1.3.1 UV/VIS Spectra

Up to a mole fraction (N) equal to 0.5 aluminum chloride, the dominant species in the melt is the AlCl_4^{-1} ion. Above $N=0.5$, a further species $\text{Al}_2\text{Cl}_7^{-1}$, controlled by the equilibrium shown below begins to appear.



At about $N=0.7$ higher polymers, $\text{Al}_n\text{Cl}_{3n+1}$ ($n>3$), may also be present. During our investigations with a series of melts ($N=0.33-0.67$), we observed that the basic melts ($N<0.5$) exhibit an absorption edge cut-off at 250 nm. The aluminum tetrachloride ion in these melts probably absorbs at about 246 nm (Figure 1).

Slightly above 0.5 ($N=0.5003$), where the molar concentration of $\text{Al}_2\text{Cl}_7^{-1}$ is approximately 0.0012, the sample showed a strong absorption peak at 282 nm. Upon addition of more aluminum trichloride, i.e., by changing the concentration of $\text{Al}_2\text{Cl}_7^{-1}$,

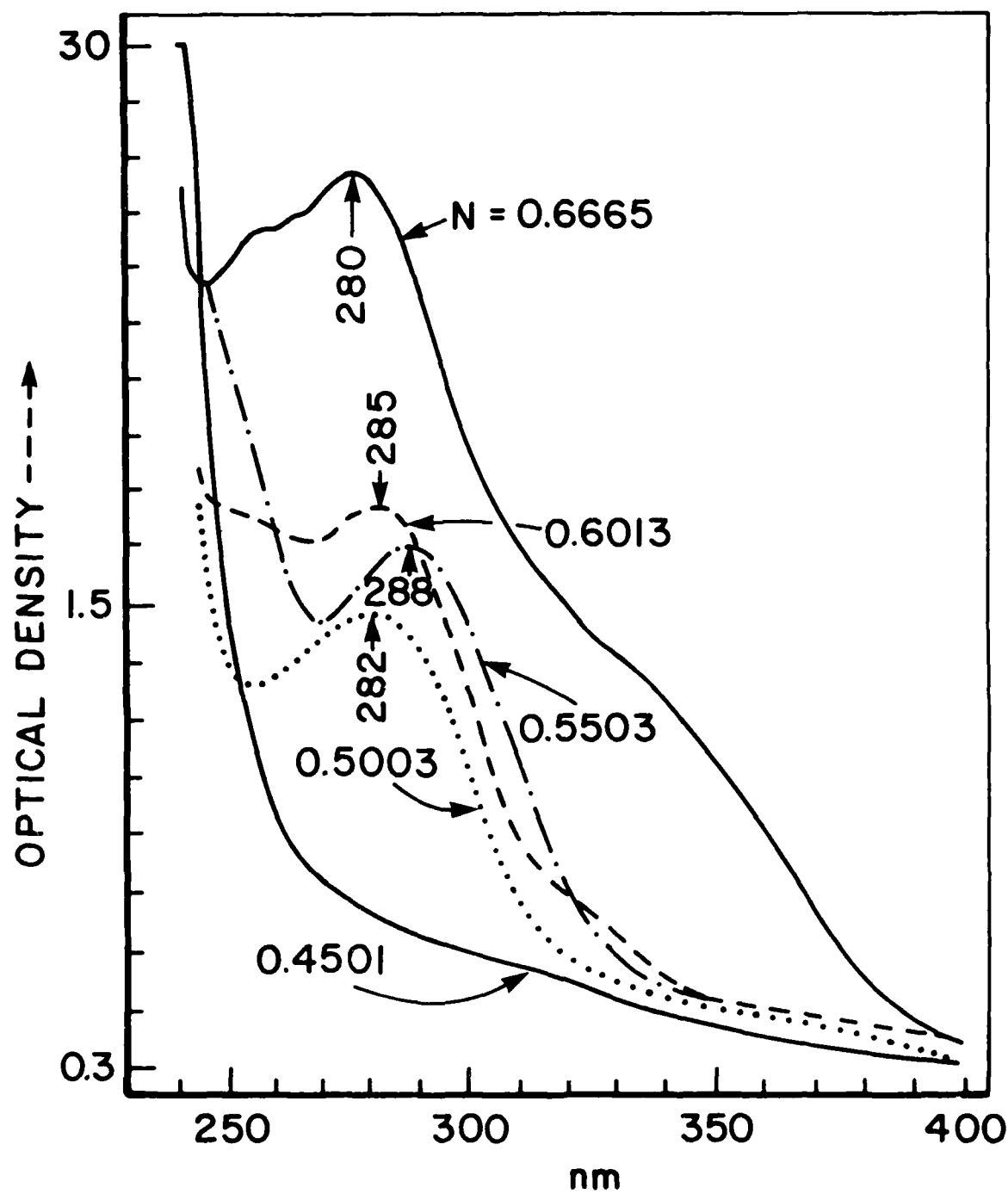


Figure 1. UV/VIS Spectra of MEIC-AlCl₃ Melts Containing Various Mole Fractions(N) of AlCl₃.

we observed an increase in the intensity of the 280 nm peak. At a mole fraction $N=0.6665$, where virtually 100% $\text{Al}_2\text{Cl}_7^{-1}$ is present (molar concentration 0.9985), we observed the maximum intensity of the 280 nm peak with a concomitant presence of a shoulder around 335 nm. The shoulder is tentatively assigned to the absorption of some higher polymers of aluminum chloride ionic specie. The results are summarized in Table 1.

These very significant observations allow us at present to identify the melt systems quantitatively in a non-destructive manner, and this method will be used in the future to characterize the modified melts.

1.3.2 Infrared and Raman Spectra

The melt samples did not lend themselves to either normal dispersive IR or FTIR investigations, because they are sealed under vacuum in 3 mm cylindrical quartz tubes, which are transparent to IR radiation only from 30-400 microns. However, the quartz is ideal for Raman spectral studies. The use of cells incorporating other types of window material, like germanium, would allow infrared studies to be made. An infrared study of the melt by conventional technique was made by sealing a smear of the melt between two CsBr plates. Figure 2 shows the infrared spectra of 0.4 and 0.6 melts. The species present in the 0.4 melt is predominately AlCl_4^- belongs to the group T_d . A group theory analysis of this symmetry group predicts two infrared active bands ν_3 and ν_4 belonging to the F_2 class (Table 2). The $\nu_4[\delta_d(\text{YXY})]$ frequency predicted to be around 180 cm^{-1} could not

TABLE 1
Ultraviolet Data on MEIC-AlCl₃ ROOM TEMPERATURE MELTS

SAMPLE	N	[Cl ⁻]	[AlCl ₄ ⁻]	[Al ₂ Cl ₇ ⁻]	OD ₂₈₅ ¹
MEICAL 1	0.3343	0.4978	0.5022	--	0.69
MEICAL 2	0.3500	0.4615	0.5385	--	0.63
MEICAL 3	0.4000	0.3333	0.6667	--	0.69
MEICAL 4	0.4501	0.1815	0.8185	--	0.66
MEICAL 5	0.5003	--	0.9988	0.0012	1.38
MEICAL 6	0.5503	--	0.7763	0.2237	1.51
MEICAL 7	0.6013	--	0.4918	0.5082	1.63
MEICAL 8	0.6500	--	0.1429	0.8571	1.03*
MEICAL 9	0.6665	--	0.0015	0.9985	2.67

¹ Optical density (OD) for a path length of 3 mm.

*It is not known why the optical density of this sample is lower than the previous ones.

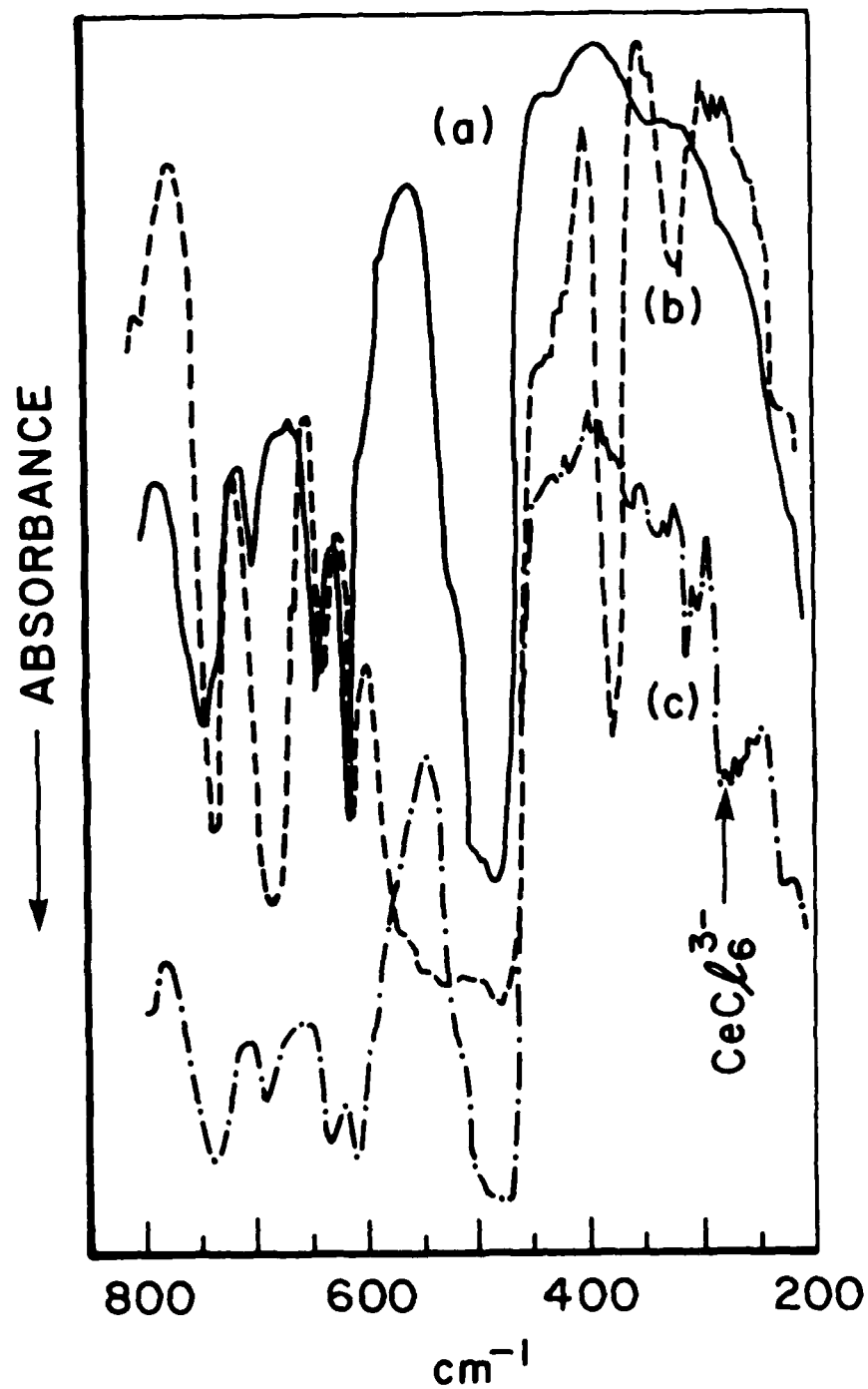
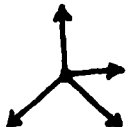





Figure 2. Infrared Spectra of (a) 0.4 Melt, (b) 0.6 Melt and (c) 0.4 Melt Containing CeCl_3 .

TABLE 2
Infrared Analysis of Tetrachloroaluminate Ion

T_d	ν_1	ν_2	ν_3	ν_4
	$[\nu_s(xy)]$	$[\delta_d(yxy)]$	$[\nu_d(xy)]$	$[\delta_d(yxy)]$
	A_1	E	F_2	F_2
	(R)	(R)	(IR, R)	(IR, R)
				
	350	120	490	180

be observed in the present case due to instrument limitation. The strong peak at 478 cm^{-1} is identified with the $\nu_3[\nu_d(XY)]$ IR active vibration in AlCl_4^- moiety present in the 0.4 melt.

The Raman spectrum of a 0.33 melt having slightly lower concentration of aluminum tetrachloride ion produced Figure 3 with the expected Raman bands at 120, 182, and 352 cm^{-1} due to ν_2 , ν_4 , and ν_1 vibrations of the AlCl_4^- moiety, respectively. The intensity distribution among these bands is in good agreement with the predicted one, 350 cm^{-1} , being the strongest.

The infrared spectrum of a 0.6 melt, containing equal amounts of AlCl_4^- and Al_2Cl_7^- exhibited two additional peaks at 378 and 320 cm^{-1} in the infrared. These peaks are due to the Al_2Cl_7^- moiety. The corresponding Raman spectrum (Figure 4) of 0.66 melt shows the 318 cm^{-1} band as the strongest with a weaker and much broader absorption around 438 cm^{-1} . These frequencies are assigned to the bridged Al--Cl--Al moiety within the Al_2Cl_7^- species. A more detailed analysis is in progress. The most significant obstacle to overcome in Raman measurements is the background fluorescence. In the present case there is no exception, all melts showed strong fluorescence. We anticipate in the near future to have available spectroelectrochemical capabilities specifically fourier transform electrochemical methods.

1.3.3 Fluorescence Spectra

Fluorescence measurements by optical (UV/near VIS) pumping often yield information on the nature of both the ground and the excited states of organic and metallo-organic complexes.

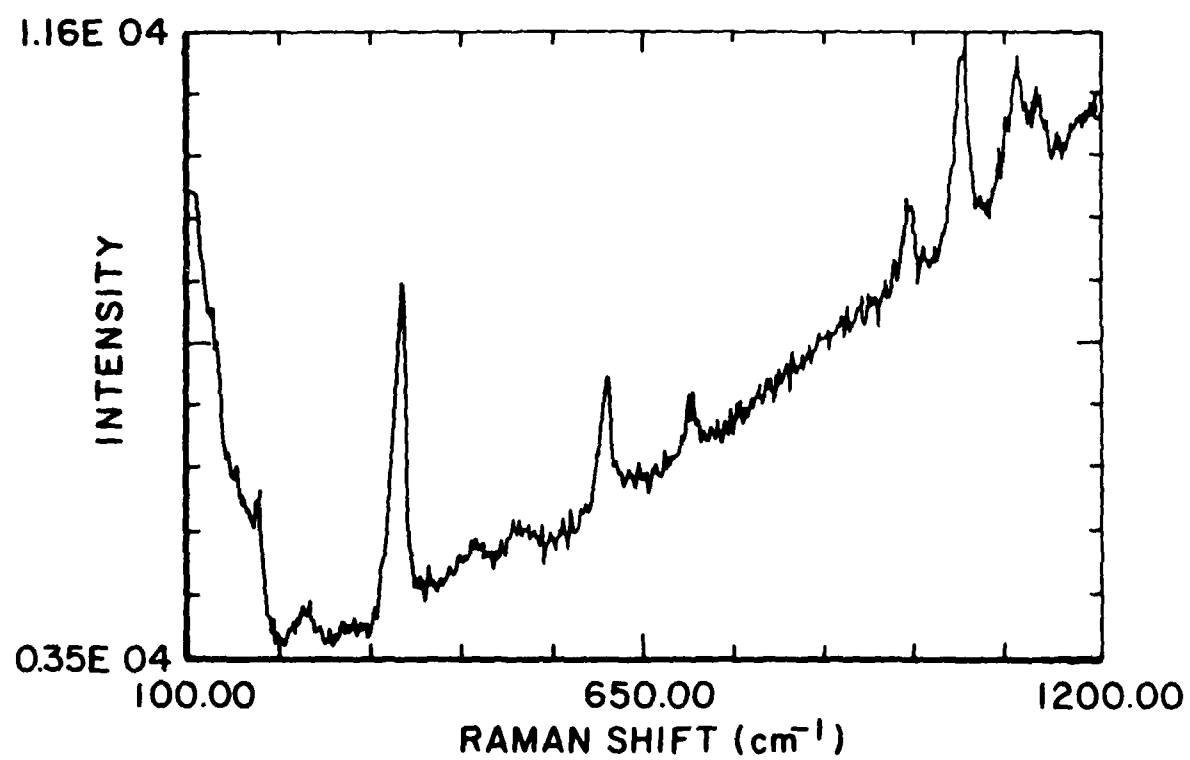


Figure 3. Raman Spectrum of a 0.33 Chloroaluminate (MEIC-AlCl₃) Melt at Room Temperature.

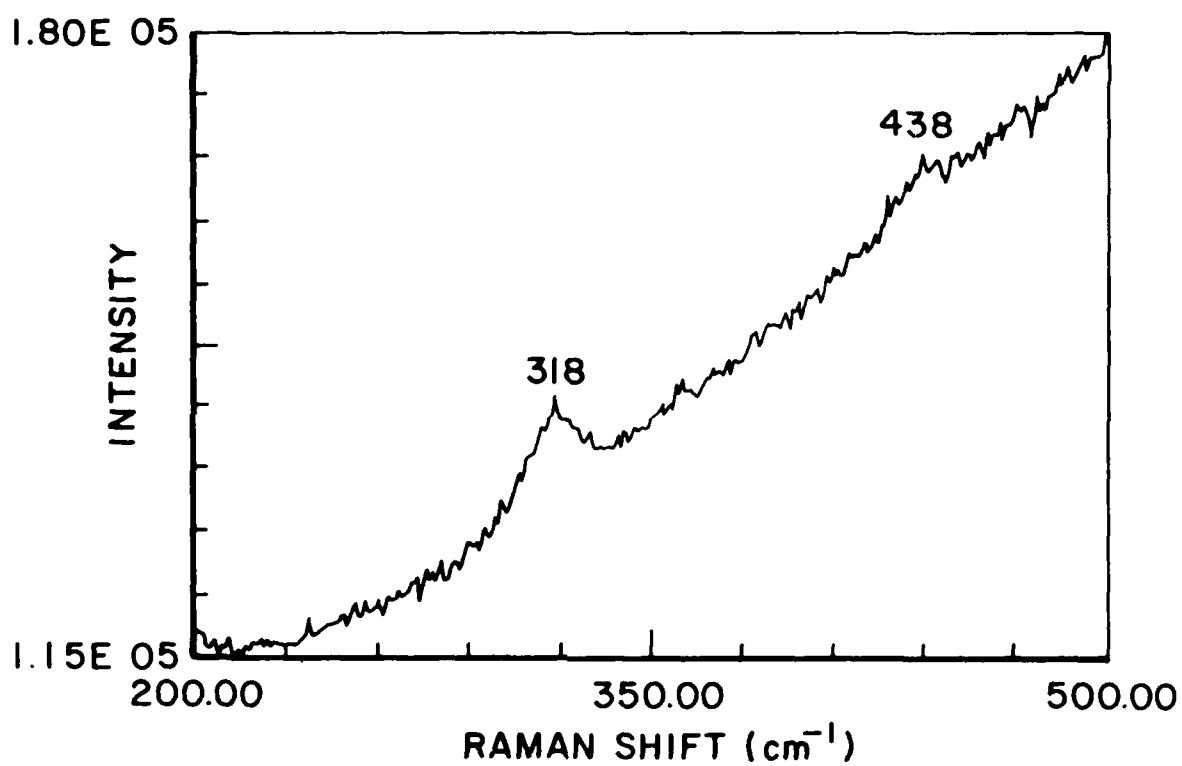


Figure 4. Raman Spectrum of a 0.66 Chloroaluminate (MEIC-AlCl_3) at Room Temperature.

This is a very sensitive method of identifying organic chromophores.

The excitation spectrum of a 0.4 melt shows excitation maxima at 270 and 395 nm with a weaker shoulder at 355 nm. These UV excitation bands are primarily due to the cationic MEIC (imidazolium cation) moiety. Excitation of the melt at these wavelengths produced fluorescence (Figure 5) which is broad and may be resolved into two components with a maxima (fluorescence) at 445 and 470 nm. The 445 nm band is easily identified as being due to the fluorescence from the organic moiety in the melt (i.e., 1-methyl-3-ethylimidazolium cation). The broader higher wavelength at 470 nm is tentatively assigned to the induced molecular luminescence from trivalent aluminum in AlCl_4^- anion. Such molecular fluorescence has been observed earlier in coordination complexes of Al(III) with organic ligands. The luminescence spectra of the lanthanides and other spectroscopic data for metal ions in the chloroaluminate melt are presented in the next section along with the electrochemical data discussed as individual ions.

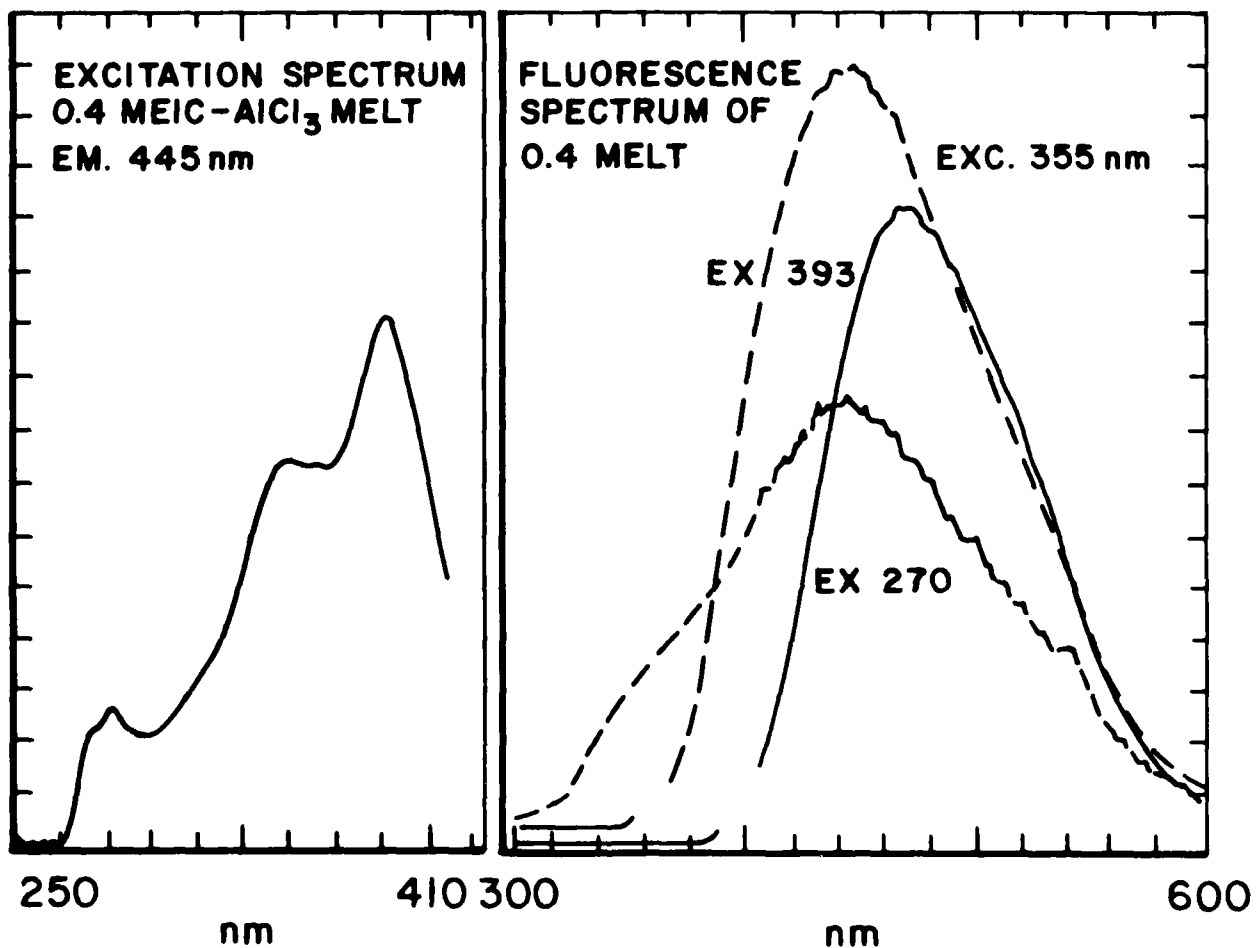


Figure 5. Excitation and Fluorescence Spectra of 0.4 Chloroaluminate (MEIC-AlCl_3) Melt at Room Temperature.

SECTION II

ELECTROCHEMISTRY

The electrochemical windows of the chloroaluminate melts (MEIC- AlCl_3) are limited by the reduction of the imidazolium cation and the oxidation of Cl^- , AlCl_4^- or Al_2Cl_7^- depending on the melt composition. Below 0.5 mole fraction of AlCl_3 , the anodic potential is strictly governed by the oxidation of free Cl^- ion and this positive limit is about 1.0 volts (Figure 6), with respect to an aluminum in 0.6(MEIC- AlCl_3) melt reference electrode. The corresponding electrochemical window of a 0.6 melt is 2.35 to -0.05 volts with respect to the same reference electrode. (2,3)

2.1 ELECTROCHEMISTRY OF CERIUM

The most extensively investigated lanthanide ion is tri-valent cerium which has a $4f^1$ electronic configuration. The E° value for the Ce(III)/Ce(IV) redox couple is strongly dependent upon the electrolytic medium used, exhibiting the effects of differing complexation of the cerium. Thus the following E° values were observed.

<u>MEDIA</u>	<u>E°(volts vs. SHE)</u>
1M HClO_4	1.70
1M HNO_3	1.61
1M H_2SO_4	1.44
2M HCl	1.28
5.5M K_2CO_3	0.05
0.4 Melt (MEIC/ AlCl_3)	0.79 ($E_p/2$)

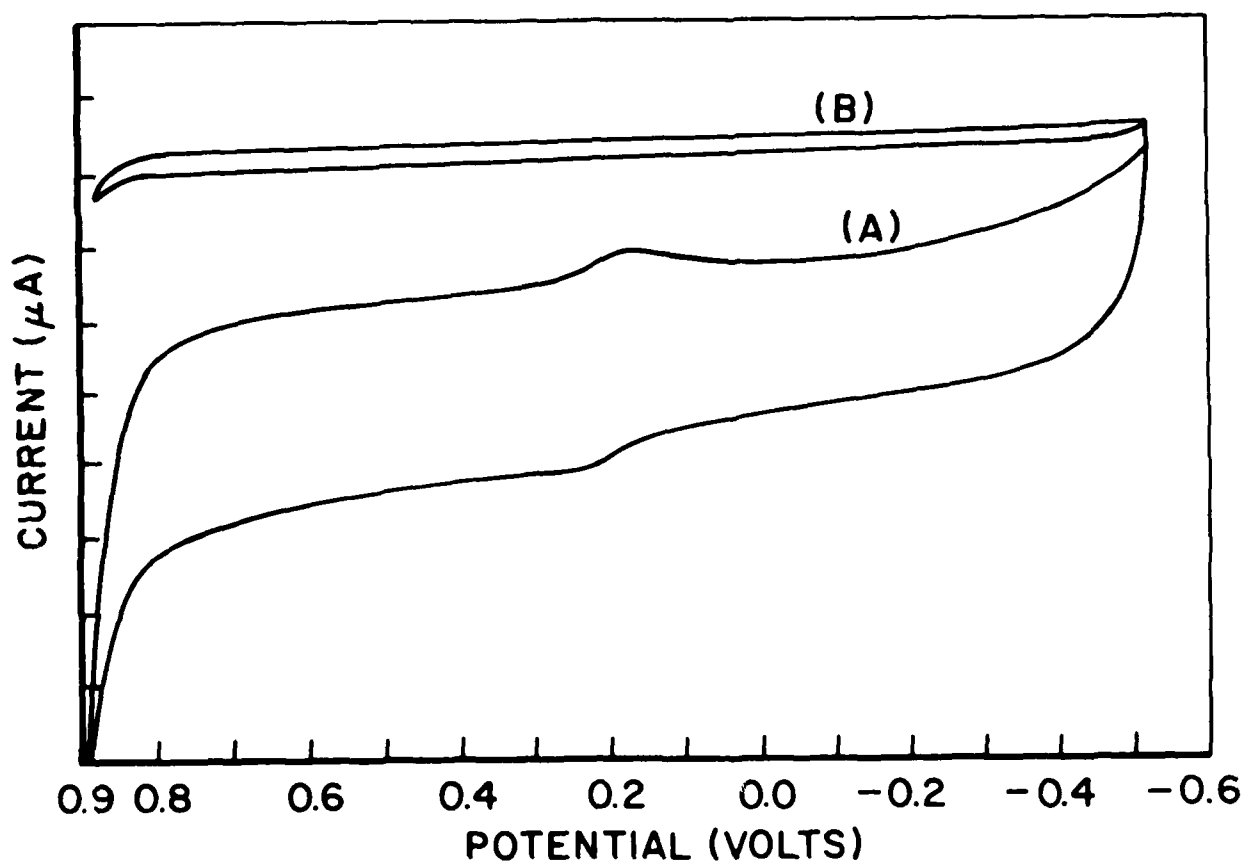


Figure 6. Cyclic Voltammogram of 0.4 Chloroaluminate (MEIC-AlCl₃) Melt at Room Temperature; 50 mV per Sec.; (A) One Microamp per Inch, (B) 10 Microamp per Inch.

The simple carbonate ion that is capable of bidentate coordination is able to lower the redox potential by about 1.6 volts from the non-coordinating ligand medium of perchlorate. The species which is probably undergoing redox reaction in carbonate medium is probably the tetra-carbonato-Ce(III) anion. From extensive spectroscopic studies Sinha established the presence of the tetra-carbonato species for all the lanthanides in aqueous carbonate solutions, having $M:CO_3^{-2}$ ratios of 1:50 at pH=12.

The cyclic voltammograms of the Ce(III)/Ce(IV) couple in 0.4 melt is shown in Figure 7. From this data we calculate the quasi-reversible rate constant of 1.20×10^{-3} cm/sec. The nature of the electroactive species was deduced from a study of the melt containing Ce(III) by UV and IR spectroscopies. The UV spectrum exhibited a strong and broad band between 310 and 350 nm. This is due to the $4f \rightarrow 5d$ type transition in Ce(III), a $4f^1$ ion. The position of the peak agreed with those observed previously for the chloro complexes of Ce(III).

The IR spectrum also showed a Ce-Cl stretching peak at 280 cm^{-1} [Figure 2(c)] in addition to the $AlCl_4^-$ peaks. The presence of peaks at 280 cm^{-1} region was found for hexachloro-complexes of cerium, thus confirming the presence of a hexachloro- Ce(III) complex within the melt. The final confirmation of the trivalent state of Ce came from the fluorescence spectral studies. As a result of exciting Ce(III) in 0.4 melt with 319 nm light, we observed a peak at 370 nm with indication of another maxima at 410 nm superimposed on the broad

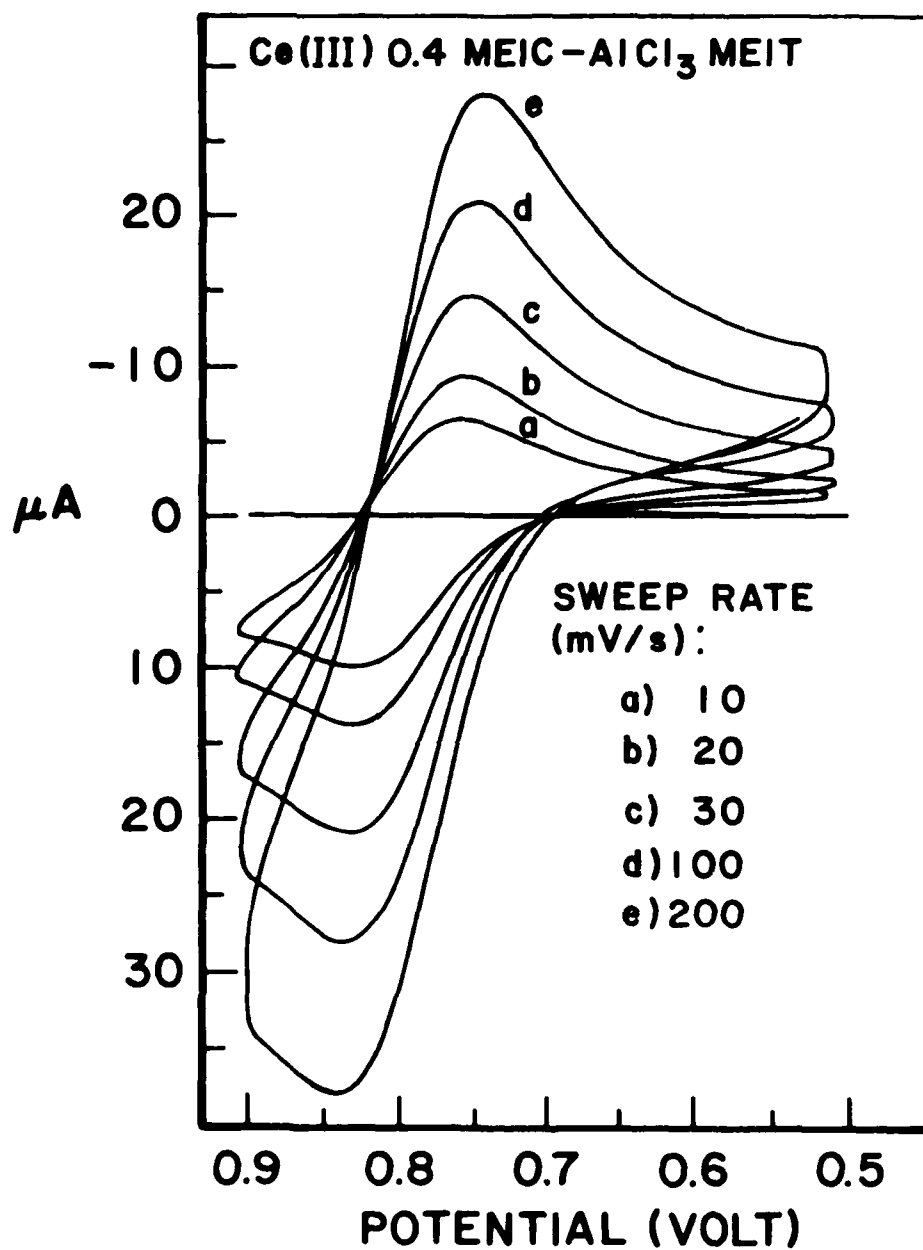
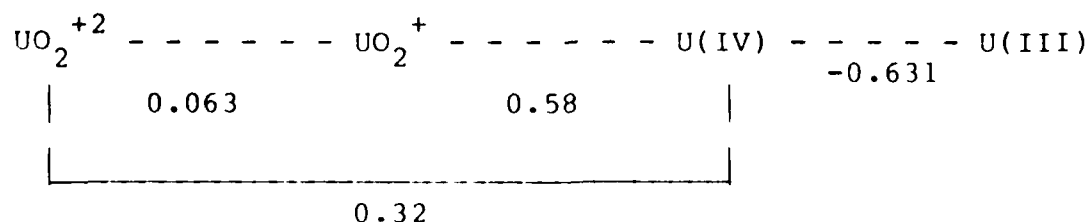


Figure 7. Cyclic Voltammogram of 0.4 Chloroaluminate (MEIC-AlCl₃) Melt Containing CeCl₃, Showing Quasi-Reversible Behavior.

fluorescence of the melt (Figure 8). The position of these peaks were further confirmed from a synchronous fluorescence study. The nature of fluorescence and the position of the peak confirmed first, the trivalent nature of Ce in the melt (0.4) and secondly, that the species is a chloro-complex. Taken altogether, the experimental data confirmed the presence of the predominant species as CeCl_6^{-3} , hexachlorocerium (III), in 0.4 melt undergoing redox reaction.

2.2 ELECTROCHEMISTRY OF URANIUM

Uranium presents an interesting challenge to the electrochemists. The oxidation states of uranium may vary between plus three and six. The usual species present are U(III), U(IV), UO_2^+ and UO_2^{+2} . In aqueous solution "naked" U(V) and U(VI) are rare. The following electrode reduction potentials are observed for aqueous solutions of uranium:



Our aim was to prepare a solution of U(IV) in 0.4 melt and study its electrochemical and spectroscopic properties. The choice of U(IV) came from the assumption that it is an interesting starting point in the above series, in that it could be reduced to the trivalent species and in the anodic wave we might be able to observe oxidation to U(IV) or possibly U(V).

Ce (III) IN 0.4 MEIC- AlCl_3 MELT

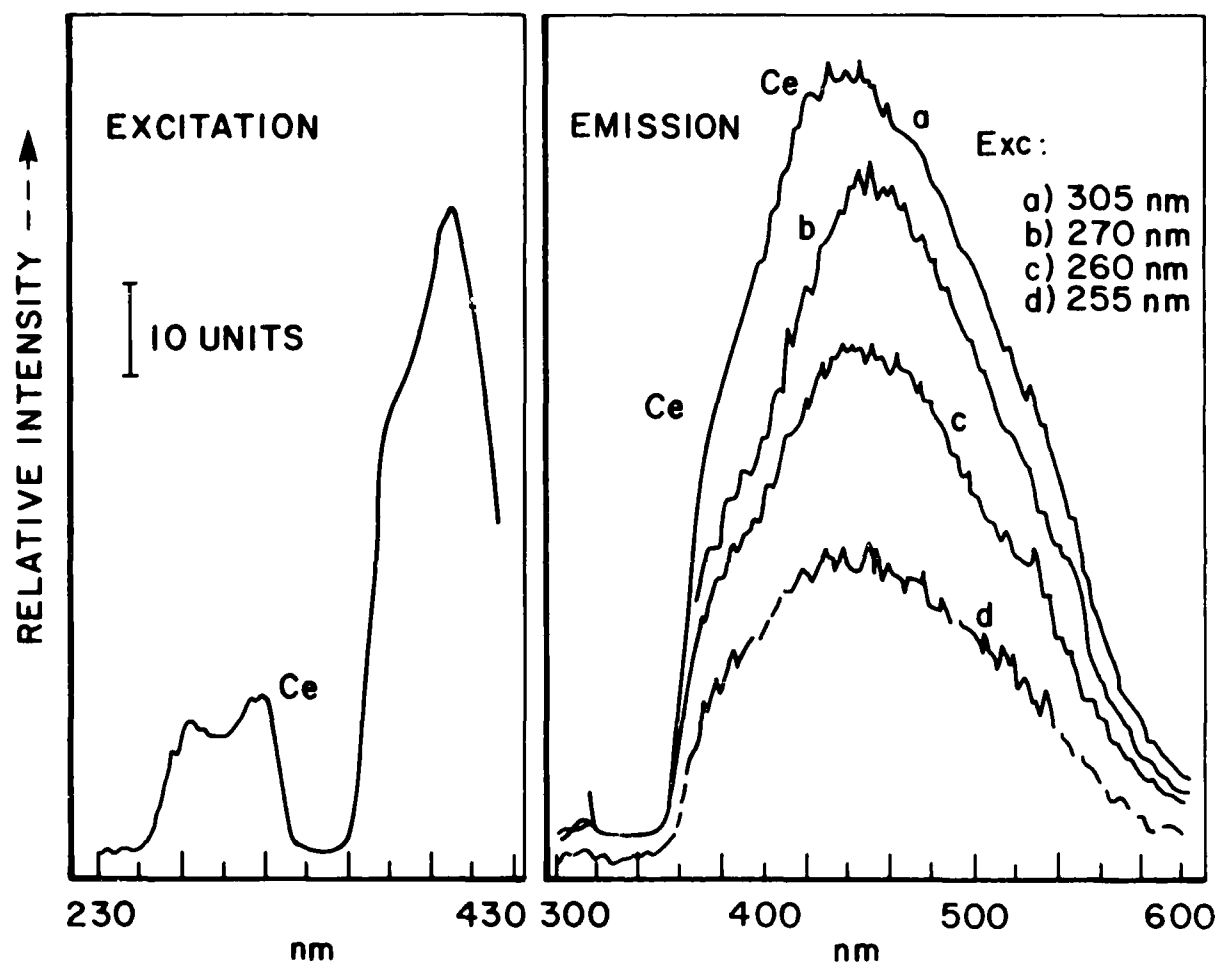


Figure 8. Fluorescence and Excitation Spectra of Ce(III) in a 0.4 MEIC- AlCl_3 Melt.

However, during the preparation of U(IV) solution in 0.4 melt we observed the change of color of "U(IV) solution" from green to yellow. Absorption spectral studies of the "yellow" solution showed no bands due to U(IV) or U(III). The yellow color is also taken as an indication of the oxidation process which may have taken place during the preparation of the melt. The following UV absorption bands were observed for the "yellow" solution: 299.5, 345.5(Sh) and 392 nm. The spectrum of the yellow liquid (Figure 9) did not show any characteristic bands due to hexavalent uranium species UO_2^{+2} .

The spectrum of our "yellow" liquid is identical with that reported⁽⁴⁾ for a nitromethane solution of $(\text{C}_2\text{H}_5)_4\text{NUCl}_6$, where the predominant species is UCl_6^- . A comparison of the spectral peak position and intensity of our "yellow" solution with $(\text{C}_2\text{H}_5)_4\text{NUCl}_6$ showed an excellent agreement and supports the point of view that the species present within the melt is predominantly UCl_6^- , an unusual U(V) species.

Cyclic voltammetric studies were performed on this unusual UCl_6^- solution. Voltammograms were obtained by scanning the glassy carbon working electrode between 0.6 and minus 1.2 volts (Figure 10). Table 3 summarizes the salient features of these voltammograms. It is apparent that the redox process is an irreversible one. The cathodic peak is due to the reduction of the U(V) specie to U(IV). The weak anodic peak current is possible due to the partial reoxidation of the U(IV) specie within the melt. If the cathodic potential is held for several minutes at

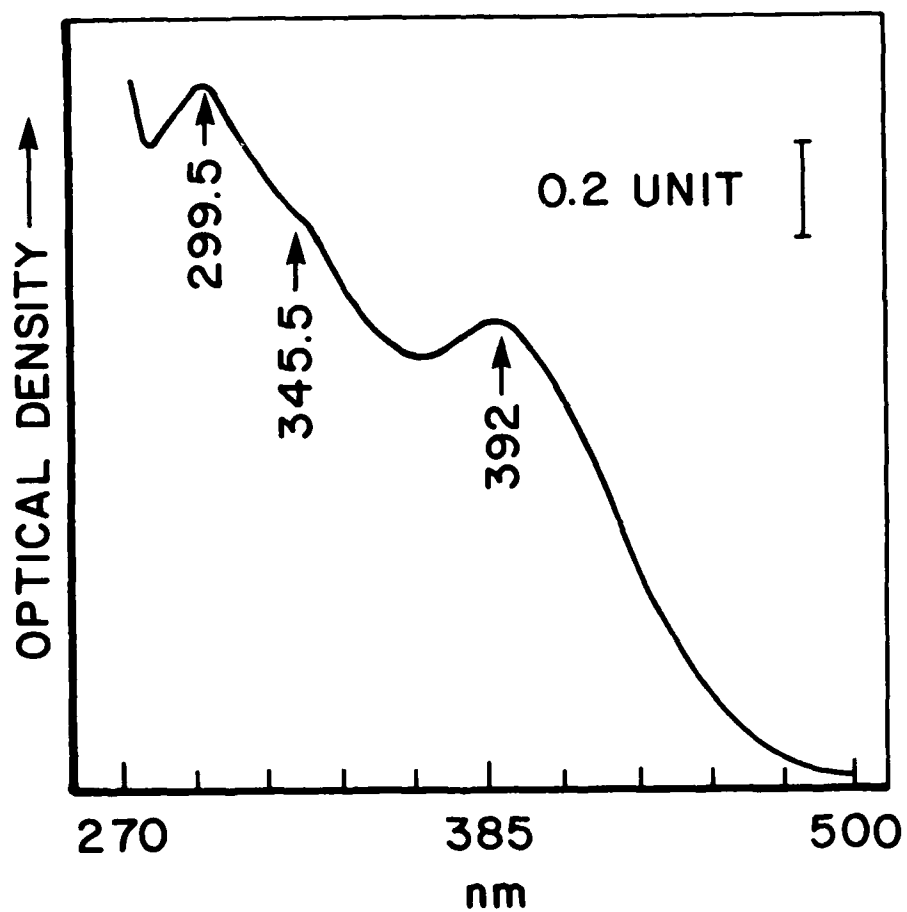


Figure 9. Ultraviolet Spectrum of the "Yellow" Solution of UCl_4 in 0.4 MEIC-AlCl_3 Melt Showing the Electron Transfer Transitions of U(V) Species.

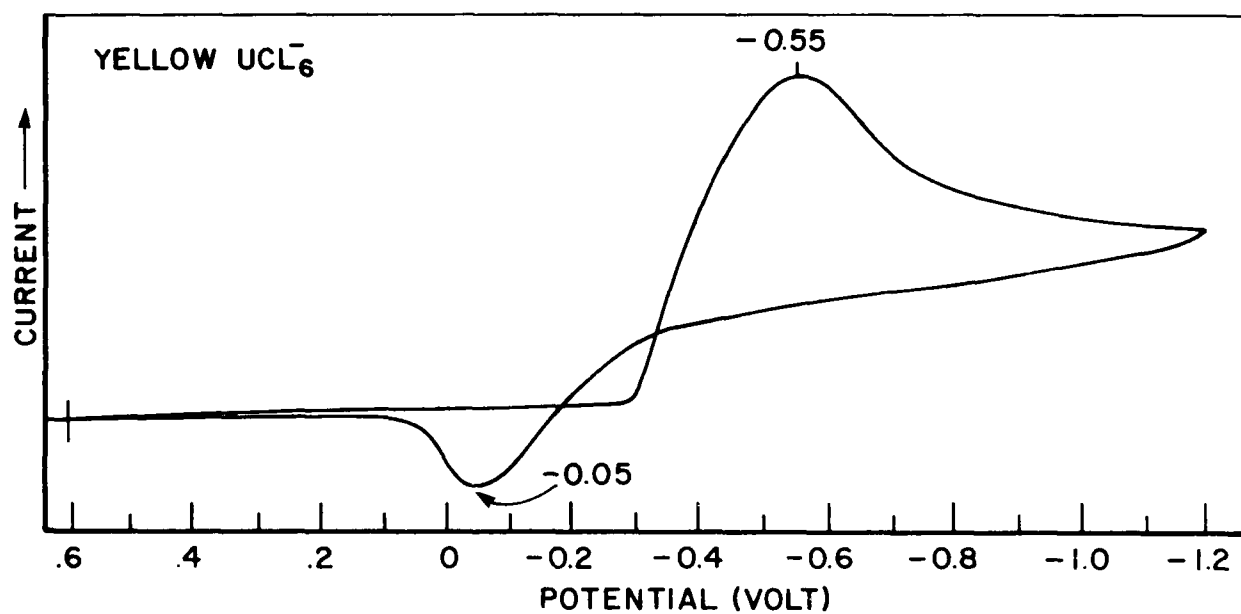


Figure 10. Cyclic Voltammetry of the "Yellow" U(V) Species Which Results From the Oxidation of a UCl_4 Solution in 0.4 MEIC- AlCl_3 Melt. Notice that the Anodic Peak is much Weaker than the Cathodic.

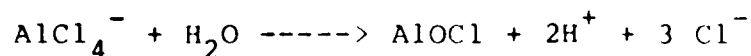
TABLE 3

Details of Cyclic Voltammetric Data on the "Yellow" UCL_6^- Solution in 0.4 Melt

ν	$E_{pc}(V)$	$E_{pa}(V)$	$\Delta E_p(V)$	$I_{pc}(mA)$	$I_{pa}(mA)$	I_{pa}/I_{pc}
700	-0.92	0.22	1.14	0.86	0.45	0.523
600	-0.88	0.18	1.06	0.71	0.37	0.521
500	-0.84	0.16	1.00	0.62	0.33	0.532
400	-0.78	0.14	0.92	0.55	0.30	0.545
300	-0.74	0.12	0.86	0.48	0.27	0.563
200	-0.66	0.08	0.74	0.40	0.24	0.600
100	-0.58	0.04	0.62	0.32	0.20	0.625
50	-0.52	-0.01	0.51	0.26	0.15	0.577
30	-0.14	-0.05	0.36	0.18	0.08	0.444

minus 0.6 volts, an almost identical current response for the cathodic and anodic wave was observed.

We now have to address the nature of the oxidizing agent present in our melt which is able to oxidize U(IV) to U(V). The species responsible is believed to be proton (H^+) which results from minute traces of water present within our melt. The water comes possibly from the water of crystallization in MEIC. Partial hydrolysis of $AlCl_4^-$ is possible with minute amounts of water according to the following equation:



The protons generated during this process should act as a strong oxidizing agent in almost anhydrous chloroaluminate melt. With yet higher concentrations of water complete hydrolysis of the tetrachloroaluminate to aluminum trichloride might result. Further work concerning the nature of water within the chloroaluminate melt and the electrochemical properties of hexavalent uranium (UO_2^{+2}) are in process.

2.3 ELECTROCHEMISTRY OF TERBIUM

Most lanthanides produce hexachloro species in MEIC- $AlCl_3$ melt (0.4). The oxidation potential of Tb(III)/Tb(IV) is too high to be measured in an aqueous solution. We have not been able to observe this redox reaction in 0.4 melt until now. However, Tb(III) was used as a fluorescence probe in 0.4 melt. From the UV, time resolved fluorescence spectrum and the excited state lifetime measurements, we suspect the presence of a

hexachloro-Tb(III) complex in 0.4 melt. A comparison of the excited state ($5D_4$) lifetime in 0.4 melt with other laser liquids and gas phase complex $[(AlCl_3) \times (TbCl_3)]$ showed the chloroaluminate melt to be a comparable, if not superior laser liquid.

LIFETIMES OF SPECIFIED SOLUTIONS IN MILLISECONDS

LEVELS	AQUO-ION	$TbCl_3-(AlCl_3)_x$	$Tb:POCl_3:SnCl_4$	0.4 Melt
$5D_3$	---	0.29(250C)	0.29(25C)	0.40(25C)
$5D_4$	0.43(25C)	1.52(250C)	2.73(25C)	2.34(25C)

2.4 ELECTROCHEMISTRY IN AQUEOUS SOLUTIONS

In order to make a comparison of the $E_{p/2}$ values of various lanthanides and U(IV), UO_2^{+2} in the melt we have started to measure the values of $E_{p/2}$ in 1 M chloride ion solutions using the same glassy carbon electrode. Figures 11 and 12 show the cyclic voltammograms obtained for Eu(III) and Sm(III) ions in 1 M aqueous chloride solution. The systems are electrochemically irreversible, as evidenced by the large separation of the anodic and cathodic peak potentials. The absence of an anodic peak for the Sm(III)/Sm(II), suggests that the Sm(II) reacts very fast with the solvent and that no Sm(II) is present within the solution to give rise to an anodic peak. These studies on aqueous solutions are in progress together with electrochemical studies within the chloroaluminate melt.

2.5 SUMMARY OF RESULTS

- a.) Studies on these melts with UV and IR spectroscopy indicate that quantitative identification of the melts are possible using these techniques.

- b.) Additional studies are necessary before a similar statement could be made regarding Raman and fluorescence spectroscopies.
- c.) The large electrochemical windows of the chloroaluminate melts are useful for studying the electrochemical properties of the lanthanides and uranium.
- d.) The Ce(III)/Ce(II) redox couple is quasi-reversible.
- e.) The U(V)/U(IV) redox couple is practically irreversible.
- f.) The Tb(III)/Tb(IV) redox process cannot be observed in the melt.
- g.) In aqueous solutions En(III)/Eu(II) is quasi-reversible but Sm(III)/Sm(II) is practically irreversible.
- h.) UV/VIS and fluorescence spectroscopies are helpful in identifying electroactive species present in 0.4 melt solutions of the lanthanides and uranium.
- i.) There is a good chance that the 0.4 melt may be useful as an anhydrous laser liquid.
- j.) A paper entitled, "Hexachloro Complex of Uranium(V) in Room Temperature Ionic Melt," by S. H. Sinha was published in Lanthanide Actinide Research 1: 195-196, 1986 (A copy is enclosed.)

2.6 SCOPE OF FURTHER STUDIES

- a.) Continued studies on the uranium system is highly desirable.

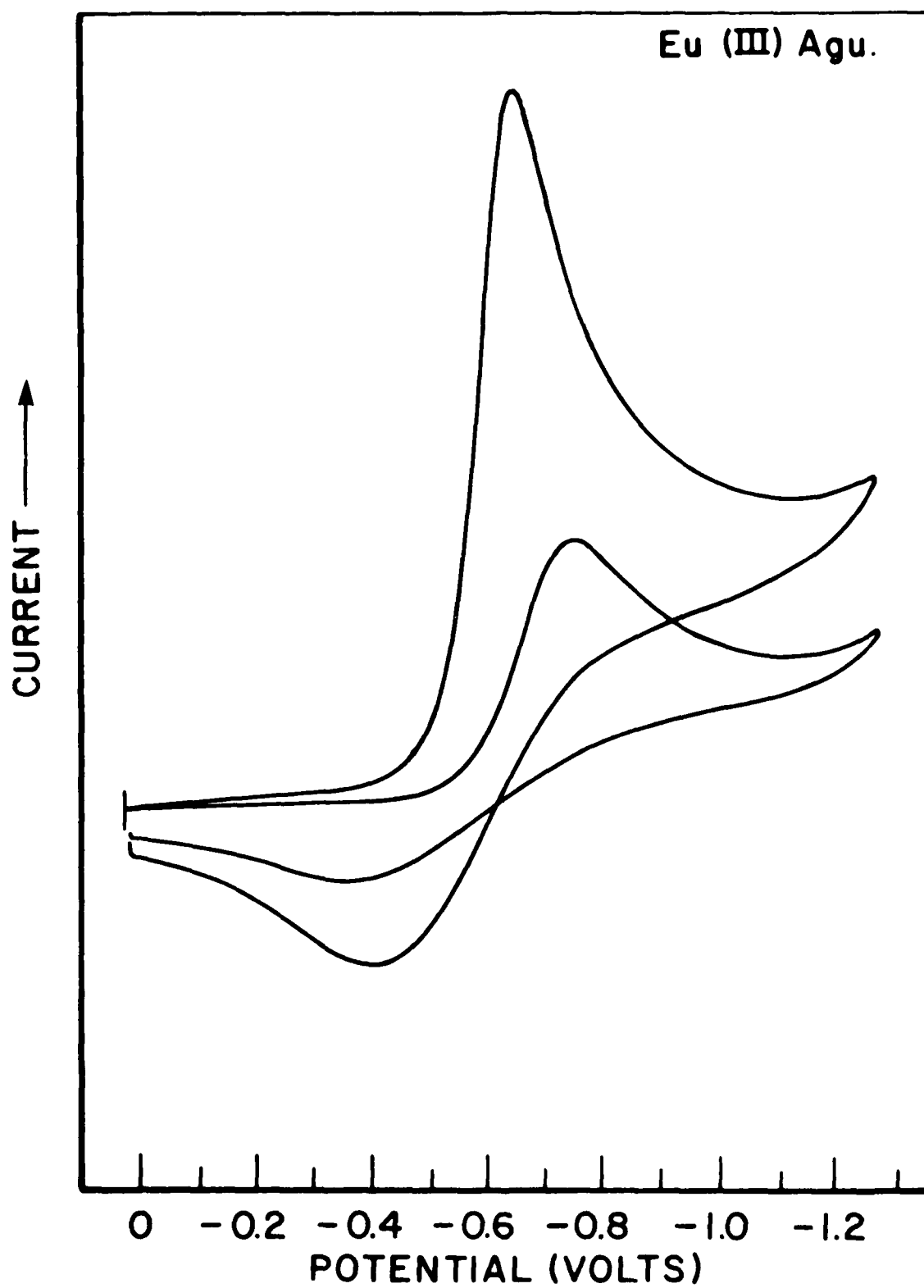


Figure 11. Cyclic Voltammetry of an Aqueous Solution of Eu(III) in 1M Chloride.

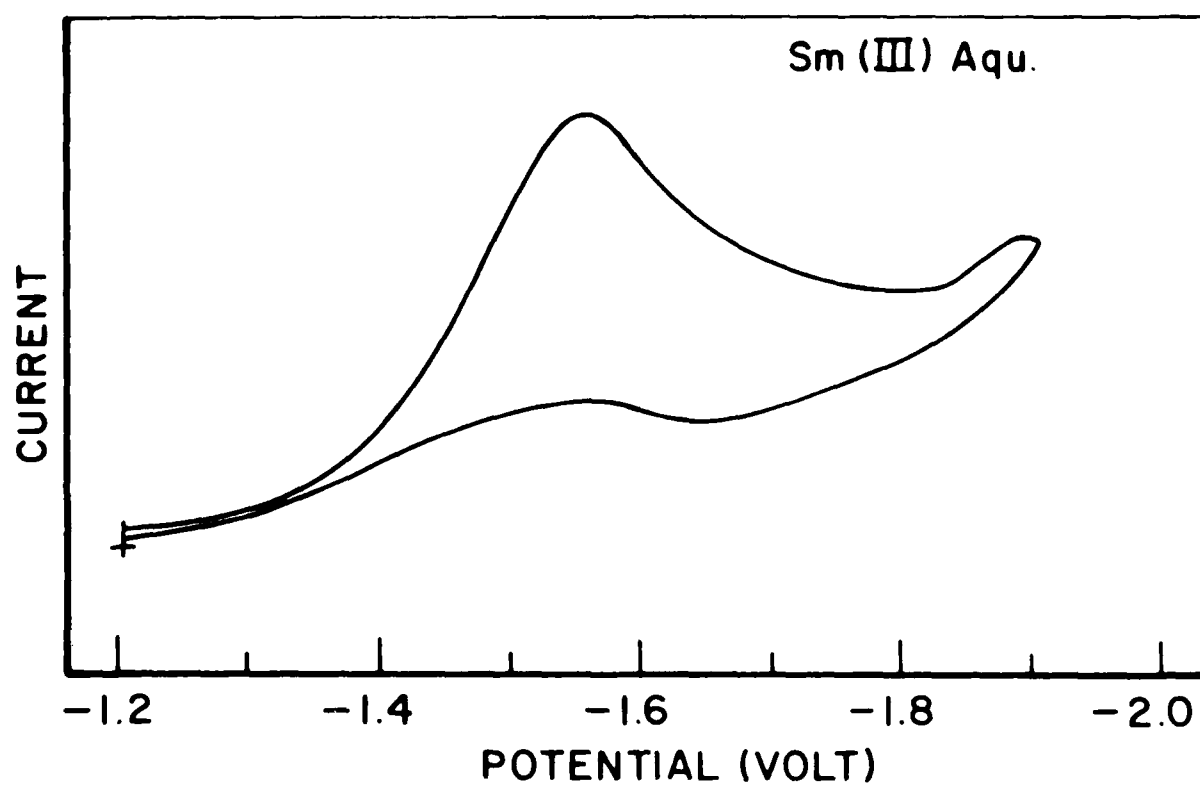


Figure 12. Cyclic Voltammetry of an Aqueous Solution of Sm(III) in 1M Chloride.

- b.) Modify the melt to widen the electrochemical window and improve the conductivity of the melt.
- c.) Studies on Eu(III) , Sm(III) , Yb(III) and UO_2^{+2} and possibly Pr(III) should be conducted.
- d.) Further studies on the use of this melt as a laser liquid deserve attention.

SECTION III

LITHIUM ELECTROCHEMISTRY IN ACETONITRILE: AN ELECTROCHEMICAL AND SPECTROSCOPIC STUDY OF ELECTRODE SYSTEMS

3.1 INTRODUCTION

Acetonitrile is well suited as a nonaqueous solvent system for electrochemical studies because of its physical properties which include its non-reactivity at many electrodes over a wide range of potentials⁽⁵⁾ and its ability to dissolve substantial quantities of salts to produce conductive solutions. The recent work by Keisele⁽⁶⁾ on the purification of acetonitrile was used as a background study for this research. The redox system of lithium in organic solvents is of interest because of the metal's attractiveness as an anode material for high-energy-density battery systems. This attractiveness is due in part to its low equivalent weight and large standard electrode potential⁽⁷⁾. Lithium reacts well as an electrode in primary battery systems, with the exception of the voltage delay problem, which results from the formation of passivation layers upon its surface. Its position as an anode for a secondary battery system is not as well understood. We believe that a very careful study should be made on behalf of the lithium acetonitrile system to determine the reasons, both energetic and kinetic which at present preclude lithium from being used as an anode within both primary and secondary battery systems. In addition, we note that little is understood about the solvation of lithium by the solvent-electrolyte and the redox processes which occur at the lithium electrode.

This portion of the research effort concerns the study of ultra-pure acetonitrile in terms of identification of its remaining contaminants, its further purification, the purification of electrolyte salts and the electrochemical behavior of lithium electrodes in acetonitrile. We hope to add to the electrochemical results spectroscopic data including spectroelectrochemical data in an effort to better understand the fundamental processes which occur in this system and to then be in a position to predict which solvent systems might be viable for battery systems of the future.

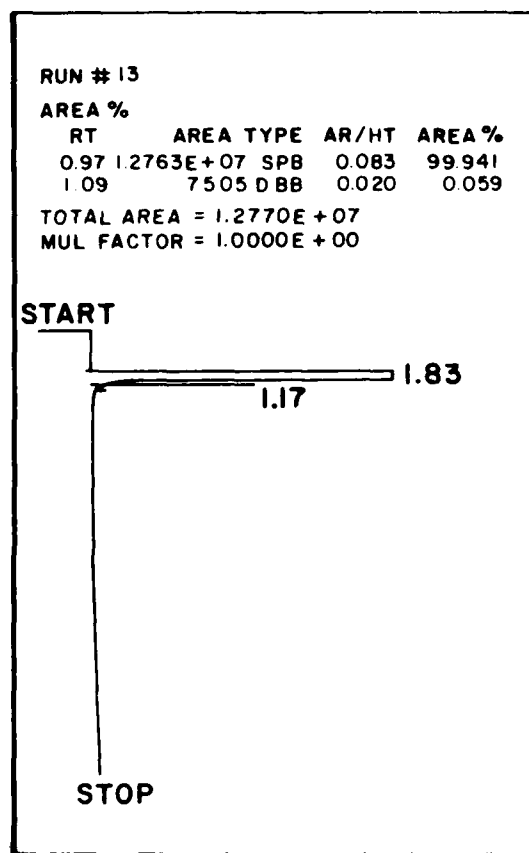
3.2 PREPARATION AND CHARACTERIZATION OF SOLVENT-ELECTROLYTES

Acetonitrile, HPLC quality or better, used in this research was obtained from Fisher, Burdick and Jackson, as well as Alfa Products. Gas chromatograms were obtained for each from a Hewlett-Packard Model 5890 capillary column gas chromatograph. We regularly used glove bags in an attempt to provide an atmosphere devoid of water vapor. These attempts were only marginally successful because we were never really certain of the chemical state within the glove bag nor were we able to document the reproducibility of the environment within these glove bags at different times. To remove whatever traces of water might remain, we passed the acetonitrile through a drierite column. Of the samples which we used, that provided by Fisher was the best, being better than 99.94+% pure as determined from capillary GC

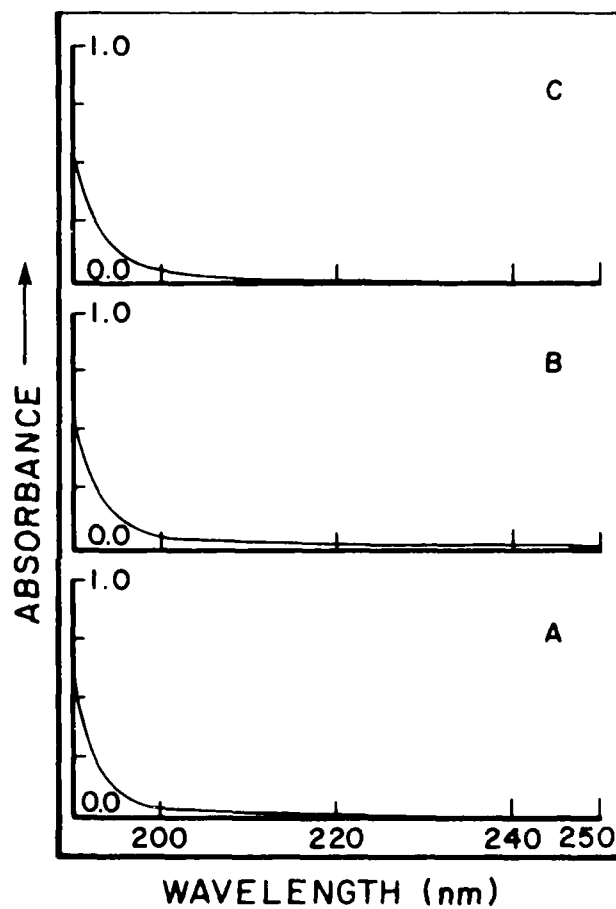
using a flame ionization detector (FID). Acetonitrile samples received from burdick and Jackson were almost equivalent to those from Fisher. By comparison, the Alfa samples contained substantial impurity. It is important to note that within the acetonitrile from all three suppliers, the only organic impurity found from our capillary GC studies was propionitrile, confirmed by deliberately spiking the sample with this compound, the next member of the homologous series. We did not consider this to be a serious contaminant, since propionitrile should have similar electrochemical properties to acetonitrile⁽⁸⁾.

The visible/ultraviolet (VIS/UV) spectra of all acetonitrile samples, obtained on a Perkin-Elmer Model 4B, were essentially identical, each being transparent down to 200 nm. Typical GC and VIS/UV traces of the Fisher acetonitrile are in Figure 13(a) and 13(b), respectively. The absence of a dry box facility has precluded us from making any definitive conclusions regarding impurity compounds, including water, which might have contaminated our solvent electrolytes during the course of our research. We have proposed that we purchase a glove box for the next phase of our work.

The electrolytes used were LiClO_4 , LiBF_4 and tetrabutylammonium tetrafluoroborate (TBATFB) from Alfa Inorganics. Each salt was dried by subjecting it to a one microtorr vacuum for at least twenty-four hours. The lithium perchlorate was also heated to 70°C. With these samples we then proceeded to conduct the electrochemical portion of the research at the lithium electrode.



(a)



(b)

Figure 13. (a) Typical Capillary Column Gas Chromatograph of Acetonitrile Showing Trace Impurity of Propionitrile.
(b) Ultraviolet Spectra of Acetonitrile Samples: (A) Fisher, (B) Burdick and Jackson, and (C) Alfa.

A quantity of TBATFB was added to the acetonitrile to act as a supporting electrolyte. Drierite was kept within the glove bag to collect any moisture as well as an indicator for the atmosphere. Normal precautions were taken. Prior to the commencement of a study, the bag, containing all necessary equipment, was purged for minutes, and sealed. After purging, a glass column was packed with alumina (Sigma Type WA-4). the acetonitrile was filtered through the column, the first several milliliters (ml) discarded and the remainder used to fill the electrochemical cell.

3.3 THE ELECTROCHEMISTRY OF LITHIUM

For these studies platinum was used for both the test and counter electrodes. The reference electrode was Ag/AgNO₃ (0.1M) in acetonitrile (AN). Cyclic voltammograms (CV) were obtained at either platinum or glassy carbon. While we could have used lithium metal as the working electrode we reasoned that in order for this solvent system to be viable, it must be capable of reducing lithium ion to its elemental state. In addition, the platinum electrode would serve as a good indicator for the presence of other redox activity within the solvent-electrolyte system prior to the addition of the lithium ion. In the absence of lithium ion, the voltage window for the acetonitrile-TBATFB system was found to be just below five volts as evidenced by the CV's at platinum (Figure 14).

Addition of lithium perchlorate to the AN-TBATFB system results in a CV which contains three peaks, (Figure 15), all

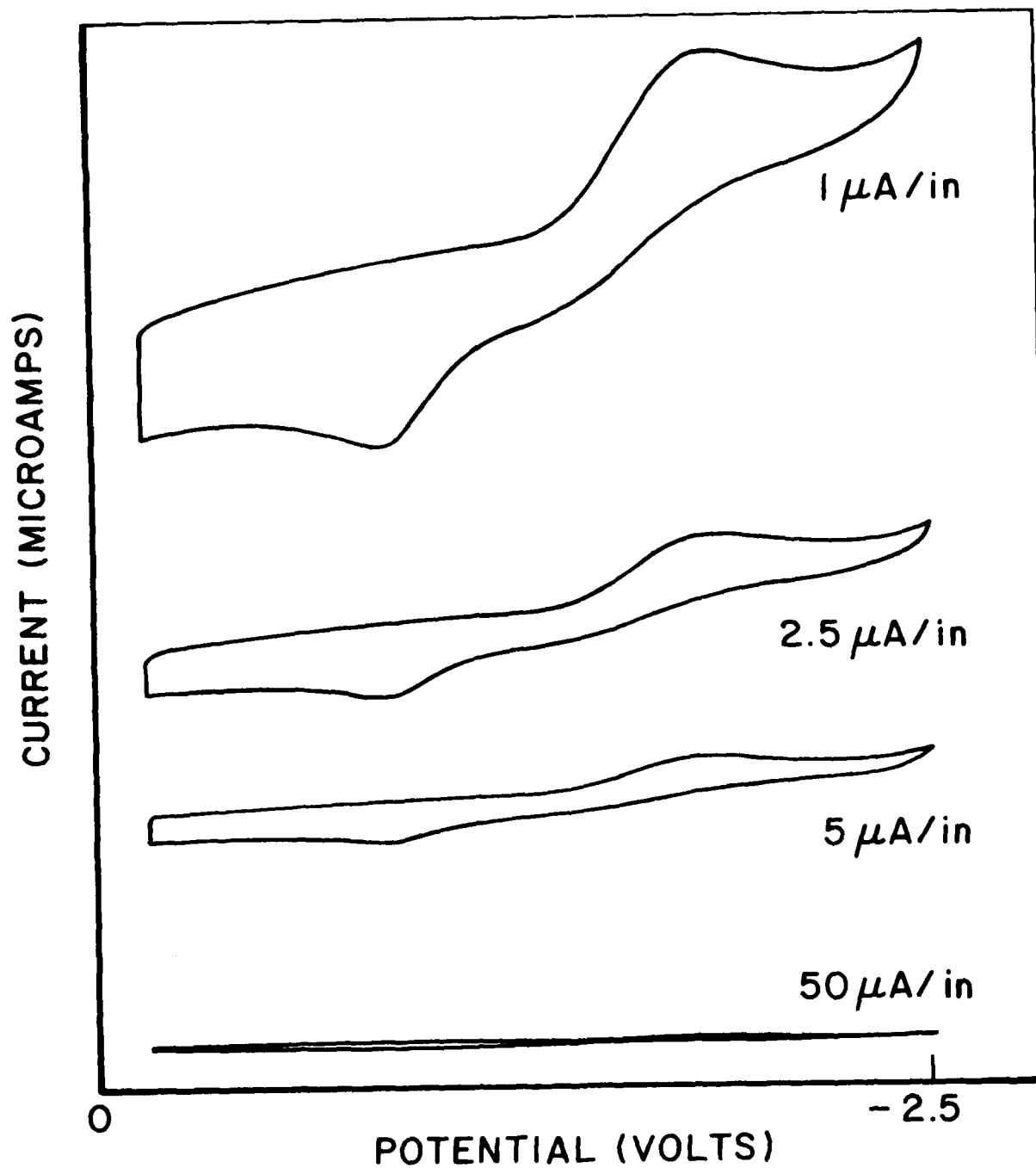


Figure 14. Cyclic Voltammogram of TBATFB in Acetonitrile at Platinum, 200mV/sec, Zero to Minus 2.5 Volts, Silver Reference Electrode, as a Function of Current Sensitivity.

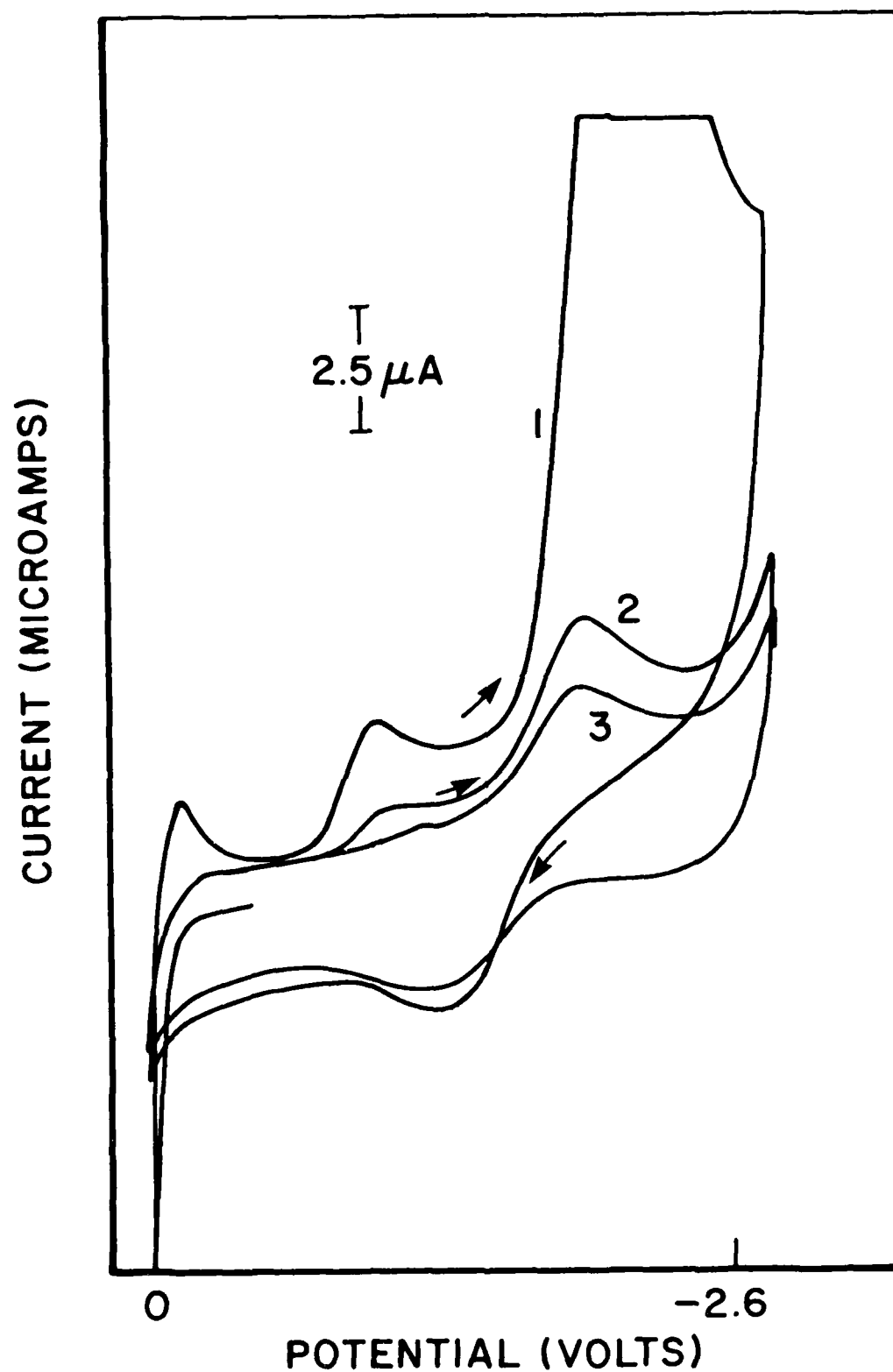


Figure 15. Cyclic Voltammogram of TBATFB and Lithium Perchlorate in Acetonitrile at Platinum, 100mV/Sec, Zero to Minus 2.6 Volts, 2.5 Microamp per inch, Silver Reference, Multiple Scan.

minus at 0.1, 0.85 and 1.85 volts versus the reference electrode. The first of these is probably due to hydrogen reduction, while the second and third are probably due to the reduction of lithium on platinum and lithium, respectively. This lithium layer, in agreement with Pons⁽⁹⁾, does passivate rapidly. The severe reduction in the reduction peaks, particularly at minus 1.85 volts, is most likely due to the formation of a passivated layer. It is interesting to note that the passivation layer which forms is soluble. This is readily shown by allowing the electrochemical cell to sit for a period of several minutes and then repeating the experiment. The CV obtained will be almost identical to that obtained from the first experiment (Figure 15). We have determined that the i_p is proportional to the square root of the sweep rate, suggesting the lithium transport process is indeed diffusion controlled. In addition, the reduction peak at minus 1.85 increases with increase in the concentration of lithium ion in solution.

SECTION IV
SUMMARY OF RESULTS

4.1 SUGGESTIONS FOR FUTURE RESEARCH

- A) Electrochemical measurements can be very useful, however, the information one could gain from spectroelectrochemical experiments could be much greater and much more definitive.
- B) We have just acquired both Raman and fourier transform infrared (FTIR) spectroscopies within the Chemistry Department at the University of Dayton. We have commenced work on electrochemical cells for spectroelectrochemical studies.
- C) We suggest that to gain some insights about the energetics of the ion solvation process that spectroscopic data in pure and perhaps mixed solvent systems be obtained.

SECTION V

REFERENCES

1. J. S. Wilkes, J. A. Levisky, R. A. Wilson, and C. L. Hussey, Inorganic Chem., 21, 1263, (1982).
2. B. P. Piersma and J. S. Wilkes, Frank J. Siler Research Laboratory Report, FJSRL-TR 82-0004, September 1982.
3. Frank J. Siler Research Laboratory Report, FJSRL-TM 83-0016, June 1983.
4. J. L. Ryan, Journal Inorg. Nucl. Chem., 33, 153, (1971).
5. A. J. Fry and W. F. Britton, Solvents and Supporting Electrolytes," in Laboratory Techniques in Electro-analytical Chemistry, Eds. P. T. Kissinger and W. R. Heineman, Marcel Dekker, New York, 1984, p. 371.
6. H. Keisele, Anal. Chem., 52, 2230, 1980.
7. H. V. Venkatesetty, Lithium Battery Technology, John Wiley and Sons, New York, 1984.
8. C. K. Mann, "Nonaqueous Solvents for Electrochemical Use," in Electroanalytical Chemistry, 3, Ed. by A. J. Bard, Marcel Dekker, New York.
9. S. Pons and S. Khoo, DTIC Technical Report, Government Accession No. AD-A106815, August, 1981.

APPENDIX
PAPERS PUBLISHED

HEXACHLORO COMPLEX OF URANIUM(V) IN ROOM TEMPERATURE IONIC MELT

Shyama P. Sinha

Department of Chemistry, University of Dayton,
Dayton, Ohio 45469, U.S.A.

During our recent electrochemical and spectroscopic investigations [1,2] of solutions of Ce(III) and Tb(III) in the room temperature chloroaluminate melt prepared by interacting 1-methyl-3-ethylimidazolium chloride (MEIC) and AlCl_3 (mole ratio 0.6:0.4, commonly known as 0.4 or basic melt [3]), we became interested in studying the U(IV) system. Spectroscopic studies of Ce(III)- and Tb(III)-containing basic melts indicated the presence of a MCl_6 -type chromophore in solution.

Dissolution of UCl_4 (Alfa Products) in the basic (0.4) MEIC- AlCl_3 melt, under dry nitrogen, occurs giving a green U(IV)-containing liquid. However, the solution bleached to a clear yellow color within a 12-hour period. Spectroscopic examination of this yellow liquid showed no absorption bands due to U(IV) nor did it exhibit the characteristic peaks of the UO_2^{2+} ion in the visible region [4].

The first low energy absorption band for this yellow liquid (Fig. 1) is observed at 392 nm (25.51 kK) with a half-width (δ) of 3.79 kK toward the lower wavenumber side, and it is indeed due to the electron transfer transition of $\text{U(V)}(5f^1)$ in our basic melt. The observed spectrum profile is identical with that reported by Ryan [5] for a nitromethane solution of $(\text{C}_2\text{H}_5)_4\text{NUCl}_6$, where the predominant species is UCl_6^- . The first electron transfer band for $(\text{C}_2\text{H}_5)_4\text{NUCl}_6$ occurs at 25.3 kK giving a value of 2.16 for the optical electronegativity (χ_{uncor}) of U(V) in the hexachloro complex. Using our experimental value of 25.51 kK for the electron transfer transition we calculate the value of χ_{uncor} as 2.15 for U(V), which is in excellent agreement with that obtained (2.16) by Ryan for the UCl_6^- complex. A comparison of our electron transfer spectrum with the closely related distorted octahedral species like U_2Cl_{10} and $\text{UCl}_6 \cdot \text{AlCl}_3$ identified in the gaseous state for a mixture of UCl_6 and AlCl_3 between 400 and 800°K [6] is not possible due to the lack of the spectrometric data on these species in the UV region.

We now have to address the nature of the oxidizing species present in our melt that is able to oxidize U(IV) to U(V). The usual impurity present in AlCl_3 is Fe(III), which may easily be involved in the oxidizing reaction. However, the AlCl_3 (Alfa Products 99.997% purity) was sublimed and the Fe(III) impurity was found to be below the limit of cyclic voltammetric detection. In our case, the species responsible for the oxidation of U(IV) is believed to be the proton (H^+) generated from the minute amount of water present as water of crystallization in MEIC and acting as a strong oxidizing agent in almost-anhydrous chloroaluminate melt. NMR and infrared studies confirmed the presence of water in the sample of MEIC and in the 0.4 melt used in this study.

Our attention was drawn to a recent study by DeWaele et al. [7] who have investigated the redox behavior of U(IV) in a chloroaluminate system similar to ours, [N-(n-butyl)pyridinium chloride (BPC)- AlCl_3], but in a melt composition of 0.33:0.66 BPC: AlCl_3 mole ratio. They believed to have found evidence of the presence of a hexachloro complex of U(V) in their melt from a study of the electronic transitions in the near IR region. It is, however, very unlikely that at their BPC: AlCl_3 ratio a considerable amount of UCl_6^- has formed. Although the observed $f \rightarrow f$ spectrum [7] is certainly due to a U(V)-chloro complex, it does not appear to be due to the UCl_6^- moiety. A more likely candidate in their melt composition is the $\text{UCl}_6 \cdot \text{AlCl}_3$ species.

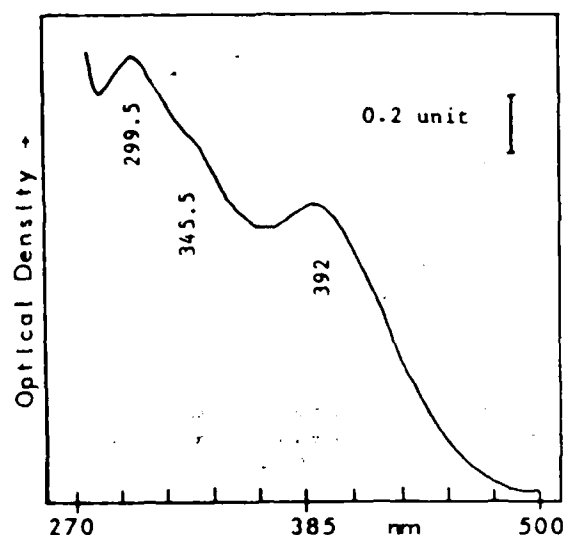


FIGURE 1. Electron transfer spectrum of U(V)-hexachloride (~ 0.035 M) in basic (0.4) MEIC- AlCl_3 melt at 25°C ; pathlength 0.2 mm.

Detailed electrochemical and spectroscopic studies on U(IV) and U(V) ions in basic and in acidic MEIC- AlCl_3 melts are in progress and the results will be reported elsewhere.

This work was performed under an Air Force Wright Aeronautics/Aeropropulsion Laboratory contract. The author wishes to thank Prof. G. Mamantov for drawing his attention to the work cited in Reference [7].

REFERENCES

1. S. P. Sinha and R. G. Keil, *Electrochem. Soc. Meeting*, Toronto, May 1985, Extended Abstract No. 542, p. 769.
2. S. P. Sinha, Paper presented at the 190th ACS Meeting, Chicago, September 1985, Inorg. Division Abstract No. 82.
3. Common Terminology: Amine chloride: AlCl_3 mole ratio 0.6:0.4, basic (0.4) melt; mole ratio 0.5:0.5, neutral (0.5) melt; mole ratio 0.4:0.6, acidic (0.6) melt.
4. J. L. Ryan, *Inorg. Chem.* 3, 211 (1964); *ibid.*, 2, 348 (1963).
5. J. L. Ryan, *J. Inorg. Nucl. Chem.* 33, 153 (1971).
6. D. M. Gruen and R. L. McBeth, *Inorg. Chem.* 8, 2625 (1969).
7. R. DeWaele, L. Heerman, and W. D'Olienlager, *J. Electroanal. Chem.* 142, 137 (1982). The labels on the wavelength scale of Fig. 8 should read 800, 1200, 1600, and 2000 nm.



Reprinted from JOURNAL OF THE ELECTROCHEMICAL SOCIETY
Vol. 133, No. 7, July 1986
Printed in U.S.A.
Copyright 1986

Resistive Electrode Effects on Cyclic Voltammetry

R. Gerald Keil*

Department of Chemistry, University of Dayton, Dayton, Ohio 45469

ABSTRACT

The effect that distributed resistance within a thin film working electrode would have upon a resulting cyclic voltammogram has been determined through simulation using the finite difference approach. Electrode resistance causes the cyclic voltammogram for a reversible electrochemical reaction to appear quasi-reversible by an amount that is proportional to the electrode resistance. The effects of the facility of the electrode kinetics and distributed electrode resistance upon the shape of the cyclic voltammogram were determined. The simulation considered mass transport by diffusion both normal and parallel to the electrode surface.

In recent times, increased effort has been devoted to technical areas which may utilize thin film electrodes, including thin film batteries, electron spin resonance cells, optically transparent electrode systems, and display devices. While the electrochemist is generally able to compensate for solution IR losses, added consideration must be given if a significant resistance is present within the electrode material itself. The results of a fundamental investigation into the interfacial energetics and charge transfer kinetics can be erroneous if solution IR losses are ignored. This is also true for a sufficiently thin metallic electrode, but, here, the magnitude of the effect will depend upon the electrode geometry as well as the number of points on the electrode to which electrical contact is made. The presence of a distributed resistance allows for

the potential at a given point in the electrode to differ from that of the potentiostat. We examine here the effects that electrode resistance and electrode geometry have upon the numerical value of ΔE_p of cyclic voltammograms for both reversible and quasi-reversible electrochemical processes. (See the List of Symbols for the definition of symbols used.)

The working electrode - Consider that a cyclic voltammogram (CV) is to be obtained at a working electrode which is composed of a long (10 cm), narrow (0.1 cm), and thin (2×10^{-3} cm) metallic film. A platinum electrode with these physical dimensions would have an appreciable resistance ($\sim 5000\Omega$). Practical considerations require in this analysis that such a film electrode have support from a nonconductive substrate. We consider further that it to manifest the extreme potentiostatic contact to the

*Electrochemical Society Active Member

electrode is made at only one end, (ii) the initial potential is sufficiently positive to preclude electrochemical reactivity; and (iii) the reaction is electrochemically reversible.

We begin with the oxidized form O of the couple present within the solution. At the commencement of the CV, the potential begins to change to less positive values. At some point, the faradaic current will become nonzero and, at that point, a voltage gradient will exist within the electrode. The change in potential at a given point in the electrode will make the potential less negative than the point at which electrical connection is made from the potentiostat. Consequently, the ratio $[R]/[O]$ at this point is also less.

The total current that passes through a given location in the electrode is a combination of the current from the portion of the electrode still further removed from this location plus the faradaic current present at this location. The exact relationship between potential, resistance, and current can be obtained if we consider the working electrode to be divided into " N " electrode elements with an equal resistance between them. The potential of the first electrode element E_1 is set by the potentiostat, but the potential of the second electrode element will be dependent upon the resistance within that element multiplied by the total current which passes through it. Therefore

$$E_2 = E_1 + R_1(i_1 + i_2 + \dots + i_N) \quad (1)$$

$$E_3 = E_1 + R_1(i_1 + i_2 + \dots + i_N) + R_2(i_2 + i_3 + \dots + i_N) \quad (2)$$

and since all R_i are equal, we can write as a general expression

$$E_i = E_{i-1} + R(i_1 + i_2 + \dots + i_N) \quad (3)$$

For sufficiently large values of either current or resistance, a given electrode element may be sufficiently positive that a faradaic process does not occur at that electrode element.

Examination of Fig. 1 shows that the resistance of a given electrode element with resistivity ρ , length Δl , and cross-sectional area $a = dw$ equals

$$R = \frac{\rho \Delta l}{a} = \frac{\rho l}{aN} \quad (4)$$

Noting that each electrode element is of width w , length Δl and has an electroactive surface area $A = \Delta l w = A/N$, one obtains as an expression for the resistance of each electrode element

$$R_i = \rho A/Nw d \quad (5)$$

Dimensionless parameters.—The analysis of resistive effects within an electrode was conducted using dimension-

less parameters. The dimensionless current at an electrode element j is given by

$$Z_j = i_j t_j^{1/2} / nFA_j CD^{1/2} \quad (6)$$

Combination of Eq. [5] and [6] gives

$$\frac{R_i i_j t_j^{1/2}}{nFA_j CD^{1/2}} = \frac{\rho A_i Z_j}{Nw d} \quad (7)$$

Noting that $A_i = A_j/N$ and $A_i = lw$ yields

$$R_i i_j = \frac{Z_j \rho n F^2 C D^{1/2}}{N t_j^{1/2} d} \quad (8)$$

Finally, division of both sides of the above expression by RT/F and utilization of the relationship $i_j = (E_i - E_{eq})/R_i$ gives as an expression for the dimensionless potential drop across a given electrode element due to the passage of current

$$\frac{R_i i_j F}{RT} = Z_j \left[\frac{\rho n^2 F^2 C D^{1/2} t_j^{1/2}}{RT(E_i - E_{eq})^{1/2} N^2 d} \right] \quad (9)$$

The quantity in brackets is the dimensionless resistance parameter, which related all quantities in the physical experiment for an electrode with rectangular geometry.

Simulation.—In this study, we considered that, initially, only the oxidized form of the redox couple is present in solution, and that the initial voltage scan will be towards more negative potentials. At the commencement of the CV, all points on the electrode surface are equipotential with the applied potential. If a nonzero faradaic current is present, the electrode elements will differ from the applied potential by an amount that depends upon the total current passing through each element as well as the direction of that current. During the negative scan, the potential of each electrode element is more positive than the contact element, as long as a nonzero current is present. With a nonzero faradaic current present, the reversal potential, E_r , is also expected to be different for each electrode element. The electrochemical events that are possible at an electrode element removed from the contact element will depend upon the potential that is present at that element. This, in turn, will depend upon the IR drop between it and the electrode element at which electrical contact is made to the potentiostat. If the potential of an electrode element is sufficiently positive, electrochemical reduction will not take place at a portion of the electrode.

An iterative numerical simulation of the cyclic voltammogram allows the I-V behavior of the electrode to be computed for a given value of the dimensionless resistance. Programs were written in Fortran IV and simulated using the finite difference approach (1-7). Typically, the program utilized several hundred iterations and up to a thousand electrode elements, the number required being a function of the dimensionless resistance. Efforts were made to minimize the number of electrode elements used and, therefore, the computing time. The number of electrode elements used was increased in multiples of one hundred until the resulting changes in ΔE_r differed less than 5% from the next smaller number of electrode elements used. Typically, a program required some 600s CPU time.

Algorithms based on Eq. [3] were used to assign a potential to an electrode element. The working electrode was divided into N elements, and each was assumed to be a thin, uniform, and continuous metallic film. Since each electrode element may have a different potential, the ratio of oxidized to reduced form at each is expected to vary. The solution phase was divided into a two-dimensional array. Diffusion, the only mass transport mechanism considered in this work, was assumed to be nonlinear, i.e., diffusion both normal and parallel to the surface of the working electrode. Capacitance effects were not included, because they are a constant, proportional to the sweep rate. An interesting and analogous problem involving so-

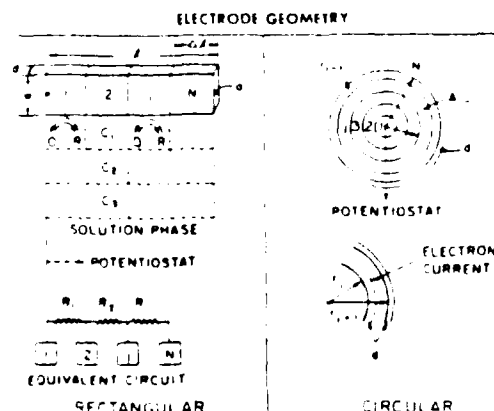


Fig. 1. Electrode geometries for rectangular and circular working electrodes.

lution resistance within electron spin resonance cells was considered previously (8) using an alternative method. The classical paper of Nicholson (9) was one of the first to yield quantitative results for the analogous solution resistance problem. The analogous problem of uncompensated solution resistive effects present in thin layer electrochemical cells was considered previously for the potential step and current step experiments using the simulation technique. The authors (10) found that nonuniform current densities resulted along the working electrode because of high electrolyte resistance. They did not consider cyclic voltammetry. The unusual current response from their simulated chronoamperometric data is seen also in our simulated CV's. We do not believe that there is any fundamental distinction between distributed resistance arising from electrode resistivity and distributed resistance arising from nonuniform current densities in solution within a thin layer cell.

The simulation commences with the assignment of the most positive potential to each electrode element and the calculation of the resulting dimensionless current at each. For the second iteration, the potential of the first electrode is again assigned, but the potential of the second electrode element and all others are computed using the total dimensionless current from the previous iteration, $Z(K-1)$. The faradaic current at a given electrode element removed from the contact electrode element may be greater or less depending upon the potential at that element relative to the standard potential for the redox process under consideration. Equations [3] and [9] show that, for the K th iteration, the dimensionless potential of electrode element j equals

$$E(j, K) = E(j-1, K) + (Z_K/RHO) \quad [10]$$

In this equation

$$Z_K = Z(K-1) \frac{N-j+1}{N} \quad [11]$$

and RHO is the dimensionless resistance parameter (Eq. [9]). For a given iteration, once the potential for a given electrode element has been assigned, the faradaic current at that element is determined, and the concentrations of electroactive components in each solution box are adjusted for diffusion. This new concentration then becomes the old concentration in preparation for the next iteration. A flow chart of the digital simulation program is shown in Fig. 2.

The results of the computer simulation of resistive electrode effects are shown (Fig. 3) for a working electrode with a dimensionless resistance equal to 15. Viewed clockwise, Fig. 3A indicates the potential of a particular working electrode element at a given time (iteration). The distributed resistance within the electrode causes the potential scan to be nonlinear. The most dramatic portion (arrow) occurs with the commencement of significant faradaic activity at electrode elements close to the contact element. For an electrochemically reversible reaction this nonlinearity will destroy the dependence of the faradaic current on the square root of the scan rate. We note further that the reversal potential, E_r , is different for each element and, similarly, that, at the completion of the positive scan, the potentials of the electrode elements are different. These effects become more dramatic with increased resistance. Figure 3B shows the current-time-potential response to the applied potentials for the first and two-hundredth electrode element. It should be noted here that the maximum dimensionless current, 0.510, exceeds the value, 0.4463, for the current function obtained for reversible charge transfer (11). We see that electrode elements removed from the first exhibit cathodic peak potentials more negative as well as anodic peak potentials more positive than in the absence of the electrode resistance. Lastly, we note that electrode resistance results in nonclassical structure (arrow) in the current function. Figure 3C combines the two previous figures, 3A and 3B, to form a cyclic voltammogram again for the contact element.

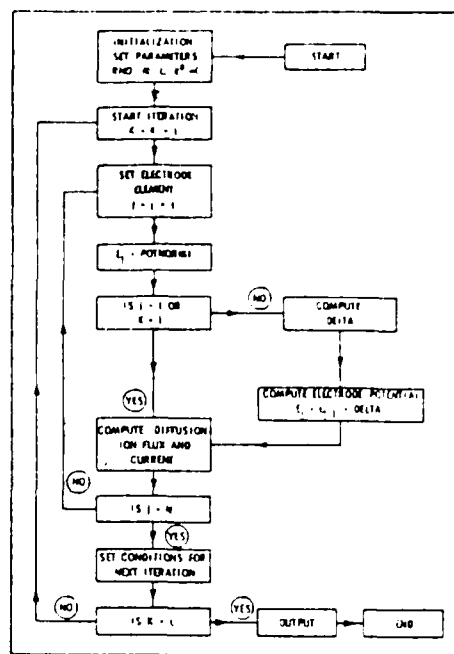


Fig. 2. Flow chart of digital simulation program

trode element and one removed. The data are presented in terms of the potential of the first electrode element. The simulation produced a marked shift in redox peak potentials and currents for electrode elements affected by resistance. Lastly, in Fig. 3D we see the cyclic voltammogram that results when the CV's for each electrode element are considered and averaged (Fig. 3D-1). For comparison, the CV obtained under identical conditions, but

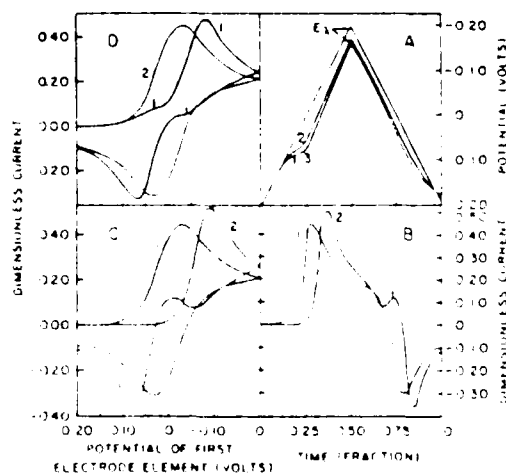


Fig. 3. Illustration of the cyclic voltammogram results obtained using the finite difference method for a facile one-electron redox reaction with resistance $\alpha = 0.5$, $E^0 = 0.0V$, $T = 298.15K$, $N = 200$, $L = 400$, $RHO = 15$. Plots A and B and Plots C and D have the same abscissa, respectively. Clockwise from first quadrant: Plot A, potential of a given electrode element: (1) contact electrode element, (2) one-hundredth element, (3) two-hundredth element. Plot B, resulting faradaic current at an electrode element at a given time (potential): (1) contact electrode element, (2) two-hundredth electrode element. Plot C, resulting cyclic voltammograms: (1) contact electrode element, (2) two-hundredth electrode element. Plot D, cyclic voltammograms: (1) average of dimensionless currents over N electrode elements, (2) for comparison, a simulated reversible cyclic voltammogram under identical conditions except that dimensionless resistance equals zero.

in the absence of resistance (Fig. 3D-2), is included. We see that the effect that electrode resistance has is to alter the shape of the resulting CV by increasing E_p , to slightly increase the peak currents, and to produce structure (arrows) as if additional electrochemical reaction(s) were possible. In a sense they are. An added peak(s) appears because the potential of electrode elements removed from the point of electrical contact lags the potential at the potentiostat.

The effect that resistance has upon ΔE_p for a reversible and a quasi-reversible electrochemical reaction is shown in Fig. 4a, in which the peak potential difference is plotted for each as a function of dimensionless resistance. The dependence appears quadratic and significant. Recalling (Eq. [9]) that the dimensionless resistance is explicitly dependent upon $v^{1/2}$, we can present the peak separation as a function of sweep rate (Fig. 4b). This result is significant as a method for the diagnosis of resistive effects within a working electrode. For a simple case, consider a redox couple whose well-established electrode kinetics at platinum are to be studied at a thin film platinum electrode. The measured peak separation would enable calculation of the resistance of the film (Eq. [9]). Alternatively, for a system under study at a thin film electrode for which neither the electrode kinetics nor film resistance have been determined, the measurement of ΔE_p at two (or more) sweep rates would allow a determination of k^0 and the film resistance to be made. Conversely, a researcher who is unaware of the effect that electrode resistance has would necessarily underestimate the value of the electrochemical exchange rate constant, k^0 .

A word of caution is necessary to those who use iterative methods of computation. The changes in the system between successive iterations must be sufficiently small to preclude oscillatory behavior. Recall that, in this analysis, we begin with the oxidized form of the redox couple present, and that we begin with a potential scan in the negative direction. Specifically, if the dimensionless resistance of each electrode element is too large, then, when significant faradaic current commences at the first electrode element, that current (times resistance) will produce at the adjacent electrode element a potential that is positive of the value it had during the previous iteration. This will result in a negative (anodic) current. This oscillatory behavior will be propagated over the N electrode elements. This effect can be circumvented in part by making N sufficiently large (Eq. [9]). We chose to use the average current from the previous iteration, $Z(K-1)$, or, alternatively, the current function from the first electrode element to compute the potential of a given electrode element for the K th iteration.

The results, to this point, have been limited to a thin film working electrode with rectangular geometry. We

next considered a thin film electrode with circular geometry (Fig. 1) and with electrical contact to the potentiostat at the center. It is obvious that the resistive problem can be eliminated by using a conductive substrate, but that was not the intent of this work. While the resistance for a material of rectangular geometry is given by Eq. [4], the corresponding resistance expression for a thin film electrode with electrical contact at the center (forming electrode elements of concentric rings) is obtained through solution of the Laplace equation (Appendix). The expression for resistance equals (see Eq. [A-9])

$$R = \frac{\rho}{2\pi a} \ln(r_p/r_c) \quad [12]$$

Using reasoning identical to that used for an electrode having rectangular geometry, it can be shown for the circular electrode that

$$\frac{R_{\text{eff}} F}{RT} Z, \frac{\rho n F^2 A C D^{1/2} (2) - 1 v^{1/2}}{2\pi a (E_p - E^0) RT n^2} \ln(r_p/r_c) \quad [13]$$

Comparison of Eq. [9] with Eq. [13] yields

$$RHO[\text{circular}] = RHO[\text{rectangular}] \frac{A(2) - 1}{2\pi l^2} \ln(r_p/r_c) \quad [14]$$

As the values of r_p and r_c increase their ratio must approach unity. Therefore, a circular electrode with a single centrally located point for electrical contact should present less of a resistance problem (Fig. 1). Our simulations have confirmed this observation.

Summary

The effects that distributed resistance within a thin film working electrode has upon a cyclic voltammogram have been determined through simulation using the finite difference approach. The effects are worse if the working electrode is long and thin, and if electrical connection to the potentiostat is made at only one end. We found that the observed effects would not be found in a circular electrode, even if very thin. The problem was simulated in terms of dimensionless parameters. The presence of distributed electrode resistance allows a nonlinearity in the triangular wave to occur, resulting in a maximum value of the dimensionless current which exceeds the current function for reversible charge transfer. Electrode elements remote from the first exhibit cathodic peak potentials more negative, as well as anodic peak potentials more positive, than expected in the absence of distributed electrode resistance. In addition, nonclassical structure within the CV was observed as a direct effect of the electrode resistance. The electrode kinetics for an electrochemically well-defined and otherwise reversible redox couple could easily be thought quasi-reversible as determined from ΔE_p . Use of two (or more) sweep rates would allow a determination of both k^0 and the film resistance to be made.

Acknowledgments

The authors wish to express their sincere appreciation to A. J. Bard and S. W. Feldberg for helpful technical discussions. The authors are especially grateful to D. H. Fritts for his interest and encouragement. This research was supported by the Aero Propulsion Laboratory, Wright Patterson Air Force Base, Contract No. F33615-81-C-2012.

Manuscript submitted Sept. 20, 1985; revised manuscript received March 13, 1986. This was Paper 403 presented at the Cincinnati, OH, Meeting of the Society, May 6-11, 1984.

APPENDIX

Resistance Properties of Thin Circular Geometries

An explicit expression for the resistance of an electrode material having circular geometry requires the solution of

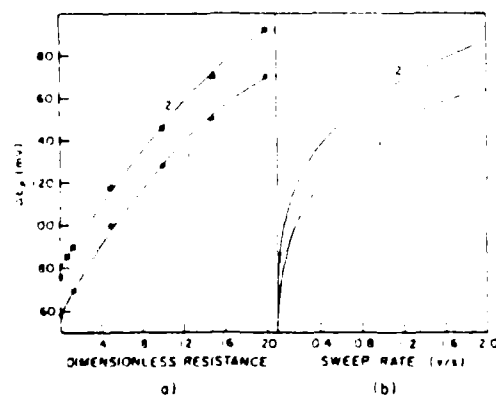


Fig. 4 Cathodic-anodic peak separation vs. the dimensionless resistance and vs. sweep rate: (1) for reversible electron transfer ($k^0 = 0.167$ cm/s, $RKS = 10$) and (2) for a quasi-reversible electron transfer ($k^0 = 6.7 \times 10^{-4}$ cm/s, $RKS = 0.40$).

the Laplace equation. In this model (Fig. 1), the electrode is of thickness d and of radius r . Electrical contact is made only at the center of the electrode. Taking the Laplace equation

$$\frac{1}{r^2} \frac{d}{dr} \left[r \frac{d^2 V(r)}{dr^2} \right] = 0 \quad [\text{A-1}]$$

integrating twice and simplifying gives

$$V_i - V_1 = C_1 \ln(r_i/r_1) \quad [\text{A-2}]$$

Therefore

$$C_1 = \frac{(V_i - V_1)}{\ln(r_i/r_1)} \quad [\text{A-3}]$$

In terms of r , where $r_1 \leq r \leq r_i$,

$$V(r) = V_1 + \frac{(V_i - V_1)}{\ln(r_i/r_1)} \ln(r/r_1) \quad [\text{A-4}]$$

The electrostatic field E equals

$$E(r) = -\frac{dV}{dr} = \frac{(V_i - V_1)}{\ln(r_i/r_1)} \frac{1}{r} \quad [\text{A-5}]$$

The charge flux is equal to the product of the conductivity and the electrostatic field

$$J_k(r) = gE = \frac{g(V_i - V_1)}{\ln(r_i/r_1)} \frac{1}{r} \quad [\text{A-6}]$$

Finally, the current is given by the integral

$$I = \int_{\omega_i} J_k(r) dA = \frac{g(V_i - V_1)}{r \ln(r_i/r_1)} 2\pi d \, dr \quad [\text{A-7}]$$

$$I = \frac{g(V_i - V_1)}{\ln(r_i/r_1)} 2\pi d \quad [\text{A-8}]$$

Using Ohm's law obtains

$$R = \frac{V_i - V_1}{I} = \frac{\rho}{2\pi d} \ln(r_i/r_1) \quad [\text{A-9}]$$

where $\rho = g^{-1}$.

LIST OF SYMBOLS

- A, electroactive surface area of j th electrode element, cm²
 A, total electroactive surface area, cm²
 a, area of electrode (end on), cm²
 C, concentration, mol/cm³
 CV, cyclic voltammogram
 D, diffusion coefficient, cm²/s
 DELTA, dimensionless electrode potential correction due to distributed resistance
 d, electrode thickness, cm
 ΔE, anodic-cathodic peak separation, mV

- E, dimensionless potential
 E_i, initial potential
 E_r, reversal potential
 E, electrostatic field, V/cm
 F, Faraday's constant, C/mol
 g, conductivity, Ω⁻¹cm⁻¹
 i, electron current, A
 i, electrochemical current, A
 J_k(r), current density, A/cm²
 j, electrode element
 K, iteration number
 k⁰, electrochemical exchange rate constant, cm/s
 L, total number of iterations
 l, electrode length, cm
 N, total number of electrode elements within electrode
 n, number of electrons
 POTNOR, dimensionless electrode potential
 R, resistance, Ω
 R_k, electrode element resistance, Ω
 RHO, dimensionless resistance
 RKS, dimensionless electrochemical exchange rate constant
 r_i, radius of i th electrode element, cm
 ρ, resistivity, Ω cm
 t_e, time of experiment, s
 T, temperature, K
 v, sweep rate, V
 V, potential, V
 w, electrode width, cm
 Z_i, dimensionless faradaic current at electrode element j
 Z(K - 1), total dimensionless faradaic current for the k th iteration

REFERENCES

1. S. W. Feldberg, *Electroanal. Chem.*, **3**, 199 (1969).
2. S. W. Feldberg, in "Computers in Chemistry and Instrumentation, Vol. 2, Electrochemistry," J. S. Mattson, H. B. Mark, Jr., and H. C. MacDonald, Jr., Editors, Chap. 7, Marcel Dekker, New York (1972).
3. K. B. Prater, in "Computers in Chemistry and Instrumentation, Vol. 2, Electrochemistry," J. S. Mattson, H. B. Mark, Jr., and H. C. MacDonald, Jr., Editors, Chap. 8, Marcel Dekker, New York (1972).
4. J. T. Malov, in "Computers in Chemistry and Instrumentation, Vol. 2, Electrochemistry," J. S. Mattson, H. B. Mark, Jr., and H. C. MacDonald, Jr., Editors, Chap. 9, Marcel Dekker, New York (1972).
5. J. T. Malov, in "Laboratory Techniques in Electroanalytical Chemistry," P. T. Kissinger and W. R. Heineman, Editors, Chap. 16, Marcel Dekker, New York (1984).
6. D. Britz, "Lecture Notes in Chemistry, Vol. 23, Digital Simulation in Electrochemistry," Springer-Verlag, New York (1981).
7. A. J. Bard and L. R. Faulkner, "Electrochemical Methods," John Wiley and Sons, New York (1980).
8. I. B. Goldberg, A. J. Bard, and S. W. Feldberg, *J. Phys. Chem.*, **76**, 2550 (1972).
9. R. S. Nicholson, *Anal. Chem.*, **37**, 667 (1965).
10. I. B. Goldberg and A. J. Bard, *J. Electroanal. Chem.*, **38**, 313 (1972).
11. R. S. Nicholson and I. Shain, *Anal. Chem.*, **36**, 706 (1964).

END
DATE
FILMED
MARCH
1988
DTIC